

FEARC-01-010

OPTIMIZATION OF BONDED PATCH TO CYLINDRICALLY CURVED SHELL STRUCTURES

Liyong Tong and Xiannian Sun

(December 2001)

DISTRIBUTION STATEMENT A:

Approved for Public Release -
Distribution Unlimited

School of Aerospace, Mechanical and Mechatronic Engineering
The University of Sydney, New South Wales 2006 AUSTRALIA

20020204 133

REPORT DOCUMENTATION PAGE

Form Approved

OMB No. 0704-0188

The public reporting burden for this collection of information is estimated to average 1 hour per response, including the time for reviewing instructions, searching existing data sources, gathering and maintaining the data needed, and completing and reviewing the collection of information. Send comments regarding this burden estimate or any other aspect of this collection of information, including suggestions for reducing the burden, to Department of Defense, Washington Headquarters Services, Directorate for Information Operations and Reports (0704-0188), 1215 Jefferson Davis Highway, Suite 1204, Arlington, VA 22202-4302. Respondents should be aware that notwithstanding any other provision of law, no person shall be subject to any penalty for failing to comply with a collection of information if it does not display a currently valid OMB control number.

PLEASE DO NOT RETURN YOUR FORM TO THE ABOVE ADDRESS.

1. REPORT DATE (DD-MM-YYYY) 29-01-2002			2. REPORT TYPE Final		3. DATES COVERED (From - To) 1 Nov 2000-31 Oct 2001
4. TITLE AND SUBTITLE Shape optimization of bonded patch to cylindrically curved shell structures			5a. CONTRACT NUMBER F6256200M9220		
			5b. GRANT NUMBER		
			5c. PROGRAM ELEMENT NUMBER		
6. AUTHOR(S) Dr. Liyong Tong			5d. PROJECT NUMBER		
			5e. TASK NUMBER		
			5f. WORK UNIT NUMBER		
7. PERFORMING ORGANIZATION NAME(S) AND ADDRESS(ES) University of Sydney Department of Aeronautical Engineering NSW 2006 Australia					8. PERFORMING ORGANIZATION REPORT NUMBER N/A
9. SPONSORING/MONITORING AGENCY NAME(S) AND ADDRESS(ES) AOARD UNIT 45002 APO AP 96337-5002					10. SPONSOR/MONITOR'S ACRONYM(S) AOARD
					11. SPONSOR/MONITOR'S REPORT NUMBER(S) AOARD-004019
12. DISTRIBUTION/AVAILABILITY STATEMENT Approved for public release; distribution is unlimited.					
13. SUPPLEMENTARY NOTES					
14. ABSTRACT Adhesive bonding is used to join or repair metallic and composite structural components to achieve or restore their designated structural stiffness and strengths. Current analysis methods and empirical databases for composite bonded patch repair or joints are limited to flat surfaces, there exists a very limited knowledge on the effect of curvature on the performance and durability of composite bonded joints and repairs. A novel finite element formulation was presented for developing adhesive elements for conducting 2.5-D simplified stress analysis of bonded repairs to curved structures. This report presents the work on optimal design of bonded composite patch using the newly developed adhesive element. Three types of design variables considered separately are (a) geo-metrical boundary shape of bonded composite patch, (b) ply drop-offs contour of bonded composite patch, and (c) fiber orientation of each ply in bonded composite patch. Sequential Linear Programming (SLP) method and one-dimensional direct search method are employed as the optimization algorithm in conjunction with a fully implemented mesh generation algorithm into which new features were incorporated.					
15. SUBJECT TERMS Adhesive Bonded Joints, Composites, Aging Aircraft					
16. SECURITY CLASSIFICATION OF: a. REPORT U		b. ABSTRACT U	c. THIS PAGE U	17. LIMITATION OF ABSTRACT UU	18. NUMBER OF PAGES
				19a. NAME OF RESPONSIBLE PERSON Thomas D. Kim	
				19b. TELEPHONE NUMBER (Include area code) +81-3-5410-4409	

FEARC-01-010

OPTIMIZATION OF BONDED PATCH TO CYLINDRICALLY CURVED SHELL STRUCTURES

Liyong Tong* and Xiannian Sun

(December 2001)

School of Aerospace, Mechanical and Mechatronic Engineering
The University of Sydney, New South Wales 2006 AUSTRALIA

ABSTRACT

Adhesive bonding has been used to join or repair metallic and composite structural components to achieve or restore their designated structural stiffness and strengths. However, current analysis methods and empirical databases for composite bonded patch repair or joints are limited to flat structures, and there exists a very limited knowledge on the effect of curvature on the performance and durability of composite bonded joints and repairs. Recently, a novel finite element formulation was presented for developing adhesive elements for conducting 2.5-D simplified stress analysis of bonded repairs to curved structures. This report presents the work on optimal design of bonded composite patch using the newly developed adhesive element. Three types of design variables considered separately are (a) geometrical boundary shape of bonded composite patch, (b) ply drop-offs contour of bonded composite patch, and (c) fiber orientation of each ply in bonded composite patch. Sequential Linear Programming (SLP) method and one-dimensional direct search method are employed as the optimization algorithm in conjunction with a fully implemented mesh generation algorithm into which new features were incorporated. Several different objective functions were proposed to optimize the bonded patch.

TABLE OF CONTENTS

ABSTRACT	II
1. INTRODUCTION	1
2. STRESS ANALYSIS USING ADHESIVE ELEMENTS	2
2.1. Review of degenerated shell elements	2
2.2. Review of adhesive element.....	3
2.3. Stress interpolation.....	5
3. SHAPE OPTIMIZATION OF A BONDED PATCH.....	6
3.1. Shape optimization method.....	6
3.1.1. Sequential linear programming	6
3.1.2. Sensitivity analysis.....	7
3.1.3 Objective function	9
3.1.4 Shape design variables	10
3.1.5. Constraints.....	11
3.2. Adaptive mesh generation	13
3.2.1. Automatic quadrilateral mesh generation [11].....	13
3.2.2 Creating a layer of offset elements along the periphery of the bonded patch.....	15
3.2.3 Improvement of the distorted elements	18
3.2.4 Mesh scheme	19
3.3 Shape optimization scheme	21
3.4 Numerical examples and discussion	22
3.4.1. Shape evolution in the optimization process	22
3.4.2. Stresses on the node and Gaussian point.....	24
3.4.3. Different objective functions	24
3.4.4. Effect of curvature.....	25
3.4.5 Composite patch.....	25
3.4.6. Optimization based on thermal stress.....	26
3.4.7. Different boundary support	27

4. OPTIMIZATION OF THE PLY DROP-OFFS OF COMPOSITE PATCH	36
4.1. Definition of the ply drop-off width.....	37
4.1.1 Ply drop-off scheme for special shape of patch	38
4.1.2. Ply drop-off scheme for general shape of patch.....	39
4.1.3. Uniform ply drop-off width.....	40
4.2. Structural analysis of the bonded composite patch with the ply drop-offs	41
4.3. Mesh scheme	43
4.4 Optimization method.....	49
4.5 Verification of the proposed FEA module	49
4.6. Numerical examples	52
4.6.1 Circular patch	53
4.6.2 Square patch	54
4.6.3 Patch with the optimum shape	55
5. OPTIMIZATION OF THE PLY LAY-UPS OF A COMPOSITE BONDED PATCH	64
5.1. Optimization method.....	64
5.1.1 Objective function	64
5.1.2 Design variables	64
5.1.3 Sensitivity analysis.....	65
5.1.4 Constraints.....	66
5.2 Numerical example	67
6. CONCLUSIONS	71
ACKNOWLEDGEMENT	73
REFERENCES	73

1. INTRODUCTION

Adhesive-bonded patching is one of the widely used repair techniques to cracked or damaged metallic and composite structures [1,2]. In this technique, a composite patch is bonded to the parent structure to reinforce the cracked zone [3] with the intent of restoring the structure to its original design specifications. This technique has successfully addressed some of the aging aircraft problems [1], and there exists a large number of research publications available on analysis, testing and design of adhesive-bonded patching repairs. A bonded patch is similar to an adhesive-bonded joint, thus the concepts and methodologies developed for analyzing stresses in bonded joints can be readily applied to conducting stress calculation for a bonded patch. There is a large amount of information on stress analysis of the bonded joints and repairs in the literature. Most of the currently available analysis methods and empirical databases for composite bonded joint design and for composite patch repair designs are limited to flat plate and/or flat laminate geometries [1, 4-6]. Compared to the knowledge of bonded joints/repairs to flat surfaces, current knowledge on the effect of curvature(s) on the performance and durability of composite bonded joints and bonded composite repairs is limited. In the first phase of this project, the effect of curvature on both peel and shear stresses in adhesive layer in adhesive-bonded curved patches was investigated by using three newly-developed adhesive elements [7,8]. In the finite element formulations, it was assumed that the peel and shear strains be constant across adhesive thickness. Some illustrative examples were also presented to demonstrate the effect of curvature on peak peel and shear stresses in the adhesive layer under selected loading and boundary conditions.

The objective of this phase of the project is to develop optimization scheme for optimum design of bonded patches. Considered are three separate sets of design variables, namely, the geometrical shape of a patch, ply drop-off (tapering) scheme and fiber orientations for each ply. Sequential Linear Programming method and one dimensional direct search method are used to optimize independently the three sets of design variables. The objective function is selected as the maximum peel stress, maximum shear stress, and maximum Von Mises stress, respectively. To facilitate mesh changes in the optimization process, an automatic mesh generator is developed to achieve a minimum the influence of shape changes on the peak objective stress. To take into account the ply drop offs, a new adhesive element scheme is

introduced to allow variation of neutral plane from element to element, which was validated by comparing with a full 3-dimensional finite element analysis using a commercial code.

2. STRESS ANALYSIS USING ADHESIVE ELEMENTS

Figure 2.1 depicts a typical curved surface with a bonded patch from one side. To optimize the bonded patch, it is essential to employ a simple and effective finite element analysis procedure. In this report, the 2.5D adhesive elements developed by the authors [7,8] are employed. In this section, a brief review the employed elements is given and a discussion on formulations for calculating nodal stresses in the adhesive layer is also presented.

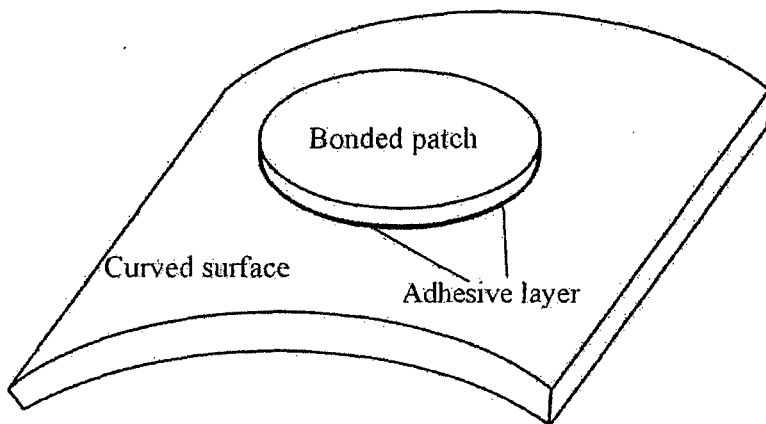


Figure 2-1 A curved surface with a bonded patch

2.1. Review of degenerated shell elements

There are two kinds of shell element for structural analysis, namely, plate-shell element and degenerated shell element. For the former one, it is based on plate element combining a drilling degree to simulate free rotation in 3-D space. However, plate-shell element is limited to cases in which all the nodes in an element must be located in one single flat plane. This introduces extra extreme difficulty to automatic mesh generator for those elements with more than 4 nodes. Although triangle plate-shell element is more attractive for this circumstance, it needs much more fine mesh to gain a satisfactory precision of stress analysis. For degenerated shell element, every node has its own nodal coordinate system and it just needs to put all the

nodes of an element in one single curved plane, which does not add any limitation to auto-meshing. Therefore, 8-node degenerated shell element with the first order shear deformation is selected to analyze both curved surface and bonded patch.

According to the first order shear deformation theory, the nodal displacements of a shell element can be defined in term of the displacements in its mid-plane in the local coordinate systems

$$\begin{aligned} U(x, y, z) &= u^0(x, y) + z\theta_y(x, y) \\ V(x, y, z) &= v^0(x, y) - z\theta_x(x, y) \\ W(x, y, z) &= w(x, y) \end{aligned} \quad (2-1)$$

where u^0, v^0, w are the translational displacements in the mid-plane of the shell, and θ_x, θ_y are the rotations of the directional normal about x and y coordinate respectively. In the shell element, each node has 5 degrees of freedom, i.e., 3 translational degrees of freedom u^0, v^0, w and 2 rotational degrees of freedom θ_x, θ_y .

2.2. Review of adhesive element

Figure 2-2 depicts a 16-node adhesive element, which consists of one pseudo-brick element modeling the adhesive layer and connecting the two shell elements. For the pseudo-brick element modeling the adhesive layer between the two shell elements, the following three basic assumptions were employed according to the characteristic of the adhesive layer:

- The patch is perfectly bonded to the curved surface with uniform thickness and no debonding occurs in the whole adhesive layer.
- The thickness of adhesive layer is very thin comparing to that of patch and curved surface. Then the strains in the adhesive layer are assumed to be uniform across the thickness of the adhesive layer.
- Only three out-of-plane stresses $\sigma_z, \gamma_{yz}, \gamma_{xz}$ are considered and other three in-plane stresses $\sigma_x, \sigma_y, \gamma_{xy}$ are assumed to be equal to zero.

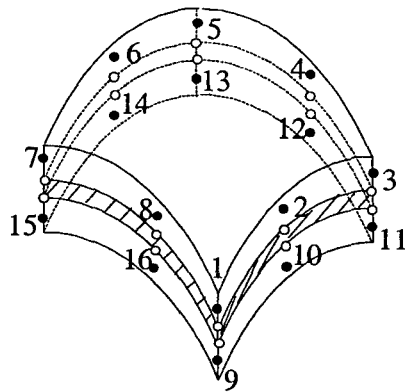


Figure 2-2 A 16-node adhesive element

Based on the basic assumptions above, the peel and two shear strains in the adhesive between pseudo-node i' and j' (see Figure 2-3) are constant and can be expressed as follows:

$$\begin{aligned}\varepsilon_{xz}^A &= \frac{1}{t}(w_i - w_j) \\ \gamma_{yz}^A &= \frac{1}{t}(v_{i'} - v_{j'}) = \frac{1}{t}(v_i^0 - v_j^0 + \frac{h_u}{2}\theta_{xi} + \frac{h_l}{2}\theta_{xj}) \\ \gamma_{xz}^A &= \frac{1}{t}(u_{i'} - u_{j'}) = \frac{1}{t}(u_i^0 - u_j^0 - \frac{h_u}{2}\theta_{yi} - \frac{h_l}{2}\theta_{yj})\end{aligned}\quad (2-2)$$

where the superscript “ 0 ” denotes the mid-plane, subscripts i and j denote the upper and lower shell elements, respectively. h_u and h_l represent the thickness of upper and lower shell elements. t is the thickness of the adhesive layer.

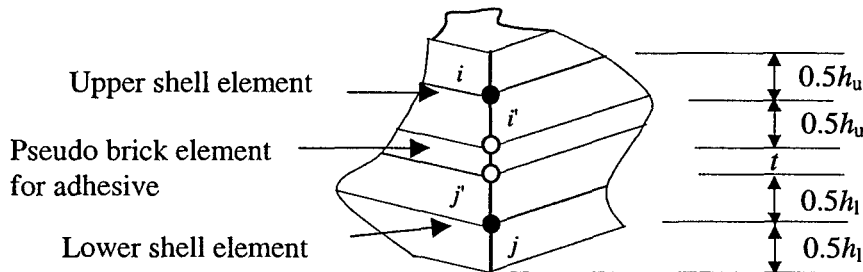


Figure 2-3 Schematic of a node pair

2.3. Stress interpolation

For an iso-parametric displacement element, the stresses at the Gaussian points have better precision, while those on the node don't possess good precision because displacements and stresses in an element have different order of continuity. Then the nodal stresses can't be obtained directly with a good accuracy. For bonded patch/joints, there always is a stress concentration near the boundary of the adhesive layer. This indicates that the stresses along the boundary are the key parameters to determine bonding strength of the adhesive layer. To overcome this drawback, a stress interpolation scheme is employed to gain the nodal stresses based on the stresses at the Gaussian points [9].

$$\begin{bmatrix} \sigma_1 \\ \sigma_2 \\ \sigma_3 \\ \sigma_4 \end{bmatrix} = \begin{bmatrix} a & b & c & b \\ b & a & b & c \\ c & b & a & b \\ b & c & b & a \end{bmatrix} \begin{bmatrix} \sigma_I \\ \sigma_{II} \\ \sigma_{III} \\ \sigma_{IV} \end{bmatrix} \quad (2-3)$$

$$a = 1 + \frac{\sqrt{3}}{2}, \quad b = -\frac{1}{2}, \quad c = 1 - \frac{\sqrt{3}}{2}$$

where $\sigma_1, \sigma_2, \sigma_3, \sigma_4$ are the interpolated nodal stresses, $\sigma_I, \sigma_{II}, \sigma_{III}, \sigma_{IV}$ are the stresses on the Gaussian point. The locations of node and Gaussian point are schematically shown in Figure 2-4.

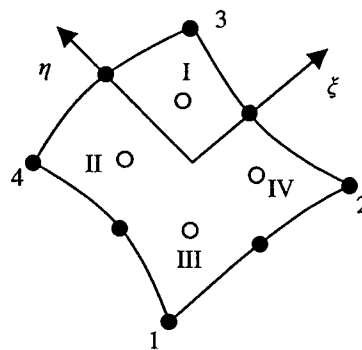


Figure 2-4 Locations of node and Gaussian point in an 8-node element

3. SHAPE OPTIMIZATION OF A BONDED PATCH

3.1. *Shape optimization method*

Sequential Linear Programming (SLP) is an effective method for shape optimization problem [10]. It concerns on linearising the objective function and constraints by sensitivity analysis and then the nonlinear optimization problem being solved by the linear programming method. In this section, we give a brief description of SLP first and then present the detailed formulations for shape optimization of the bonded patch.

3.1.1. *Sequential linear programming*

A structural shape optimization problem can be described as the minimization of an objective function subject to a number of prescribed constraints. It may be stated mathematically as

Minimize $f(X)$

Subject to
$$\begin{cases} h_i(X) = e_i & (i = 1, \dots, p) \\ g_j(X) \leq b_j & (j = 1, \dots, m) \end{cases} \quad (3-1)$$

Where $f(X)$ is the objective function, $h_i(X)$ and $g_j(X)$ represent the equality and inequality constraint functions, X is the design variable vector which contains n design variables, and p and m are the total number of equality and inequality constraints, respectively.

The optimization formulation as above is nonlinear in general. The linearization of the formulation is a must if the linear programming is going to be employed to solve the problem. The linearized formulation becomes

$$\text{Minimize } \sum_{k=1}^n \frac{\partial f}{\partial x_k} \Delta x_k$$

Subject to

$$\begin{cases} h_i(X^0) + \sum_{k=1}^n \frac{\partial h_i}{\partial x_k} \Delta x_k = e_i \quad (i = 1, \dots, p) \\ g_j(X^0) + \sum_{k=1}^n \frac{\partial g_j}{\partial x_k} \Delta x_k \leq b_j \quad (j = 1, \dots, m) \end{cases} \quad (3-2)$$

where X^0 represents the current design vector and Δx_k is the difference between two successive values for the k th design variable.

In this way, the nonlinear constrained optimization problem is transformed into a linear one. There are many methods to solve this linear inequality system, such as simplex method, which is used in this report.

3.1.2. Sensitivity analysis

For SLP, a major part of analysis cost is sensitivity analysis. In the current analysis, the structure is analyzed by displacement-based finite element method and thus all the sensitivities can be obtained by calculating the difference of displacements before and after the change of every shape design variable. Therefore, it is necessary to calculate the displacement change with a shape design variable being changed. To avoid repeating the time-consuming solution of stiffness equation, the concept of force derivative is employed to obtain all the displacement sensitivities by one single analysis, which can be found in [10], as follows.

In a finite element analysis, we have stiffness equation

$$Kq = P \quad (3-3)$$

where K is the assembled stiffness matrix, q is the vector of displacement parameters and P is a (nodal) force vector (vectors).

For a small change Δx_i of shape design variable x_i , we have

$$(K + \Delta K)(q + \Delta q) = P + \Delta P \quad (3-4)$$

Substituting equation (3-3) into equation (3-4), we obtain

$$K\Delta q = \Delta P - \Delta Kq - \Delta k\Delta q \quad (3-5)$$

Ignoring the higher order term in equation (3-5) and dividing by Δx_i on both sides yields

$$\frac{\Delta q}{\Delta x_i} = \frac{K^{-1}(\Delta P - \Delta Kq)}{\Delta x_i} \quad (3-6)$$

The term on the right hand side of the above equation is known as the force derivative of shape design variable x_i . The differentiation of stiffness and load in equation (3-6) can be calculated by

$$\begin{aligned} \Delta K &= \int_{\Omega_2} B^T D B d\Omega - \int_{\Omega_1} B^T D B d\Omega \\ \Delta P &= \int_{\Omega_2} N^T p d\Omega - \int_{\Omega_1} N^T p d\Omega \end{aligned} \quad (3-7)$$

where Ω_1 and Ω_2 represent the domains before and after the variation of the design variable x_i (see Figure 3-1). B and D are the geometrical matrix and elastic matrix of an element, respectively.

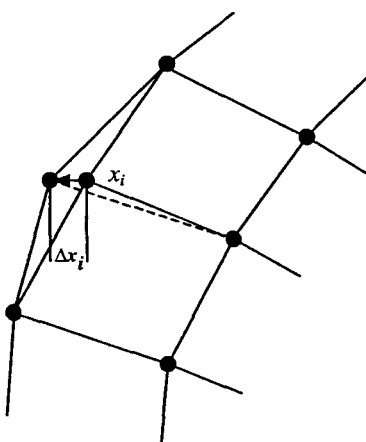


Figure 3-1 Effect of changing a design variable on the boundary of elements

To get more accurate stress sensitivities, we use the displacement change directly instead of the force derivative in this report, which is given by

$$\frac{\partial \sigma}{\partial x_i} = \frac{\sigma(q + \Delta q) - \sigma(q)}{\Delta x_i} \quad (3-8)$$

The numerical examples show that the above equation can provide an improved stress sensitivity analysis.

3.1.3 Objective function

High stress concentration occurs at the boundary of the adhesive layer and it is essential to minimize the peak stresses in the adhesive layer by shape optimization. Then, the maximum stress, which determines the strength of the adhesive layer, should be selected as the objective function. However, the failure modes of the adhesive layer depend on the material property and the load applied. Therefore, as a parametric discussion, three kinds of maximum nominal stresses are chosen as the objective function in the current analysis, and they are the maximum peel stress, the maximum shear stress and the maximum Von-Mises stress, which are defined as follows:

$$(a) \text{ The maximum peel stress } \sigma_z \quad (3-9)$$

$$(b) \text{ The maximum shear stress } \tau = \sqrt{\tau_{yz}^2 + \tau_{zx}^2} \quad (3-10)$$

$$(c) \text{ The maximum Von Mises stress}$$

$$\tau = \frac{1}{6} \sqrt{(\sigma_x - \sigma_y)^2 + (\sigma_y - \sigma_z)^2 + (\sigma_z - \sigma_x)^2 + 6(\tau_{xy}^2 + \tau_{yz}^2 + \tau_{zx}^2)} \quad (3-11)$$

According to the basic assumption for the adhesive layer, we have $\sigma_x = \sigma_y = \tau_{xy} = 0$.

Therefore, the Von Mises stress can be written as

$$\tau = \frac{1}{6} \sqrt{2[\sigma_z^2 + 3(\tau_{yz}^2 + \tau_{zx}^2)]} \quad (3-12)$$

For the sake of convenience, an equivalent stress is used in the analysis

$$\tau_{eq} = \sqrt{\sigma_x^2/3 + (\tau_{yz}^2 + \tau_{zx}^2)} \quad (3-13)$$

3.1.4 Shape design variables

Figure 3-2 depicts one quarter of a symmetric bonded patch that is mapped into x - y plane. Some points along the periphery of the bonded patch are selected to define the boundary shape of the patch. The movements of these points are assumed to be in both the x - and y -direction. At the point where $x=0$ or $y=0$, the movement is limited in one single direction, i.e. y -direction or x -direction only.

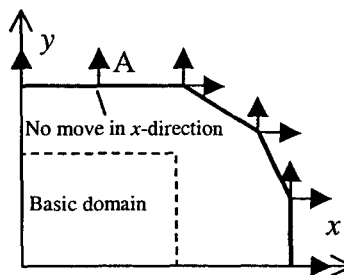


Fig.3-2 shape design variables

At certain stage, the shape change with the movement of boundary point is very small and this movement should be neglected in the current iteration. In Figure 3-2, the movement at point A in x -direction can only slightly change the shape of the patch so that it can be ignored. Therefore, only the movement in y -direction is considered at this point in the current optimization step. The magnitude of shape change can be evaluated by calculating the area change of the patch in the analysis.

It is worth noting that all the movements of shape design variables must take place in the curved surface. In this analysis, we map the patch into a flat plane and work out the magnitude and direction of shape change. Then the patch is mapped back into the curved surface.

3.1.5. Constraints

The constraints for shape optimization of bonded patch mainly concern with restraints on the objective function, move limits and other design requirement, such as weight and basic shape constraints.

Firstly, the objective function should not be increased for each optimization step. In other words, the maximum nominal stress in the adhesive layer must be smaller than that before a shape change is introduced.

Based on the sensitivity analysis described in Section 3.1.2, we have the stress gradients for every design variable. Then the stress change at a point with a shape change can be approximately evaluated by

$$\Delta\sigma_i^{(k)} = \sum_{j=1}^n \nabla\sigma_{ij}^{(k)}(x_j^{(k)} - x_j^{(k-1)}) \quad (i = 1, \dots, m) \quad (3-14)$$

Where $\nabla\sigma_{ij}^{(k)}$ is the sensitivity vector of the j th design variable at the i th node in the k th (current) optimization step, $x_j^{(k)}$ is the j th design variable vector in the current iteration, and $x_j^{(k-1)}$ the j th design variable vector in the last optimization step. m is the number of nodes where the maximum nominal stress in the adhesive layer occurs. n is the number of the shape design variables.

So the stress constraints can be expressed as

$$\sigma_i^{(k-1)} + \Delta\sigma_i^{(k)} = \sigma_i^{(k-1)} + \sum_{j=1}^n \nabla\sigma_{ij}^{(k)}(x_j^{(k)} - x_j^{(k-1)}) < \sigma_{\max}^{(k-1)} \quad (i = 1, \dots, m) \quad (3-15)$$

where $\sigma_i^{(k-1)}$ denotes the nominal stress on the i th node in the last optimization step. $\sigma_{\max}^{(k-1)}$ is the maximum nominal stress in the last optimization step.

According to the current knowledge of stress distribution in the adhesive layer, stress concentration only occurs along the periphery of the bonded patch. So only the stresses on those nodes along the periphery of the bonded patch are considered in equation (3-15). This will enable us to employ a much less number of inequality constraints for the problem considered.

The change of the maximum nominal stress with a shape change, i.e., the objective function, can be accordingly given by

$$\Delta\sigma_{\max}^{(k)} = \sum_{j=1}^n \frac{\partial\sigma_{j\max}^{(k)}}{\partial x_j} (x_j^{(k)} - x_j^{(k-1)}) \quad (3-16)$$

where $\sigma_{j\max}^{(k)}$ is the maximum nominal adhesive stress with the j th shape design variable $x_j^{(k-1)}$ being moved to $x_j^{(k-1)} + \Delta x_j$. Here Δx_j is the small change of shape design variable used in the sensitivity analysis.

Secondly, a set of constraints is imposed on the range of Δx admissible in any iteration so that every shape change can be kept in a linear range. The choice of the move limits is very important to economy and success of the optimization solution. If the move limits are made too small, the convergence will be very slow; if they are too large, oscillation may occur. The move limits can be given as

$$x_j^{(k-1)} - d < x_j^{(k)} < x_j^{(k-1)} + d \quad (3-17)$$

where d is the move limits.

From the viewpoint of engineering design, the weight of the structure is an important factor for structural design. In general, we need to keep the weight in a certain range. For current shape optimization, the weight control is implemented by applying a limit on the area of the bonded patch. On the other hand, the shape of the patch may reduce infinitely in some

direction to become a very narrow strip. To avoid this bad shape, it is necessary to define a basic domain that the shape change must take place out of this domain (see Figure 3-2). Then we also have some extra structural constraints as follows

$$\begin{aligned} A_l < A < A_u \\ x_j > x_{bj} \end{aligned} \quad (3-18)$$

where A is the current area of the patch, A_u and A_l are the upper and lower limit of area of the patch, respectively. x_{bj} is the minimum length of design variable x_j according to the limit of basic domain.

3.2. Adaptive mesh generation

It is inevitable that mesh topology varies during the optimization process due to a large shape change of the bonded patch. To avoid excessive element distortions and unreasonable large aspect ratios, even unreal element, an adaptive mesh generation algorithm should be employed to generate quadrilateral element.

In the current analysis, we assume that the curved surface is a cylindrical surface. Then a two-dimensional mesh generator is suitable for the requirements.

The basic idea of adaptive mesh generation is to map the whole structure, including the cylindrical surface, the bonded patch, and the adhesive layer, into a flat plane. Then an automatic, two-dimensional finite element mesh generator using quadrilateral elements is employed to obtain the mesh topology. Finally, the mesh in the flat plane is projected back to the cylindrical surface. Because the cylindrical surface can be easily mapped into a flat plane, it is shown that the present mesh generation scheme is very efficient and effective.

3.2.1. Automatic quadrilateral mesh generation [11]

The finite element method requires that the domain of interest be subdivided into a mesh of discrete elements. The accuracy and the expense of the calculations are strongly affected by

the ‘goodness’ of the underlying mesh. An ideal mesh is characterized by small elements where stress gradients are high, larger elements where stress gradients are small and elements that are regular or undistorted in shape.

The mesher used here is based on the ‘looping algorithm’ first described by Schoofs et al [11] and improved by Talbert and Parkinson [12]. The detailed algorithm for this method can be found in [12]. We just give a brief description here.

In this algorithm, the boundary geometry is defined in a continuous closed loop at first. Then the size of element on the boundary is specified as per preferred refinement at different locations throughout the mesh. According to a definition of visible nodes (to avoid the splitting line falling outside the concave loops), the best splitting line linking two visible nodes in a closed loop is determined by (see Figure 3-3)

$$SL = c_1\theta + c_2L + c_3\varepsilon \quad (3-19)$$

where θ is the deviation of the split angles from the ideal ($\pi/2$), L is the length of the splitting line and ε is the error in element size matching (node placement by predefined element size gradient and refinement coefficient). c_1, c_2, c_3 are constants used as weighting values and the following values were proved to give the best results [11]

$$c_1 = 0.5, c_2 = 0.3, c_3 = 0.2 \quad (3-20)$$

Based on equation (3-19) and (3-20), the original boundary is split recursively until all loops contain either four or six nodes. A six-node loop closure is processed separately.

Finally, the Laplacian method is used to smooth the mesh generated, which can significantly improve the distorted elements.

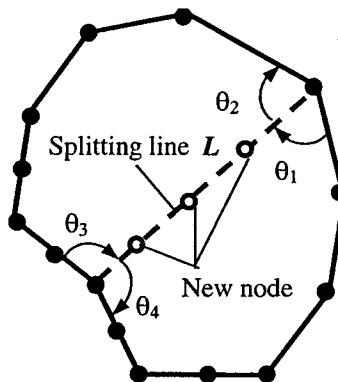


Figure 3-3 Splitting line

3.2.2 Creating a layer of offset elements along the periphery of the bonded patch

It is well known that high stress concentration occurs along the periphery of the bonded patch. Therefore, to minimize the stress concentration in this region, it is necessary to have a couple of layers of similar offset elements along the boundary of the bonded patch, which should be as square as possible, to improve the accuracy of stress analysis. Furthermore, the size of these offset elements should be kept as close to a constant as possible during optimization.

The offset element defined in this way will benefit the numerical analysis in three ways. Firstly, the distance from the boundary of the adhesive layer to the Gaussian point, where we can evaluate the adhesive stresses, only changes slightly for different shape of the bonded patch. Then it is reasonable to compare the stresses on the Gaussian point before and after shape change of the bonded patch. Secondly, it can reduce the nodal stress error caused by the change of element size. Thirdly, the total number of nodes will not change dramatically because the number of automatically generated nodes depends on the size of element predefined on the boundary by user. Thus it avoids generating too many nodes, which may result in an unacceptable long computing time for the solution of stiffness equation.

An approach to generate a layer of offset elements has already been presented in [12], which is listed in Table 3-1 as case 1-3. However, this method is based on the element size being small enough to avoid some special cases, such as two adjacent interior angles are smaller

than 120° . In the current analysis, the boundary of bonded patch changes arbitrarily with the shape evolution and it is inevitable to have these cases occur in order to keep a nearly constant element size along the boundary of patch. Therefore, some extra mesh generation methods are presented in this analysis to fulfill the requirement of the stress analysis, which are given in Table 3-1 as case 4-6. Figure 3-4 depicts the detailed configuration for all 6 cases.

The method described above can successfully generate a layer of quadrilateral offset elements along the boundary of the patch. But it may fail to generate one more layer of offset elements because the element sizes are changed on the new boundary. However, we can interpolate the generated offset elements to two layers of offset elements with aspect ratio 1:2, as shown in Figure 3-5.

Table 3-1 Offset node generation schemes

Case	Interior angle	How the offset node is generated
1	$120^\circ \leq \alpha \leq 240^\circ$	Along a bisecting line of the interior angle at a distance equal to the element size at that node
2	$\alpha \leq 120^\circ$	As the resultant of the two vectors which point to the two adjoining nodes
3	$\alpha \geq 240^\circ$	Same as case 2 except the negative of the resultant is used
4	$\alpha_1 \leq 120^\circ, \alpha_2 \leq 120^\circ$ α_1, α_2 are two adjacent interior angles	Compare the two angles, the small one is processed as same as case 2, while the big one is processed as case 1
5	$\alpha_1 \geq 240^\circ, \alpha_2 \geq 240^\circ$ α_1, α_2 are two adjacent interior angles	All two angles are processed as same as case 1
6	$\alpha_1 \leq 120^\circ, 120^\circ \leq \alpha_2 \leq 240^\circ, \alpha_3 \leq 120^\circ$ $\alpha_1, \alpha_2, \alpha_3$ are three continuous angles	Along a bisecting line of α_2 at a distance equal to the element size at that node

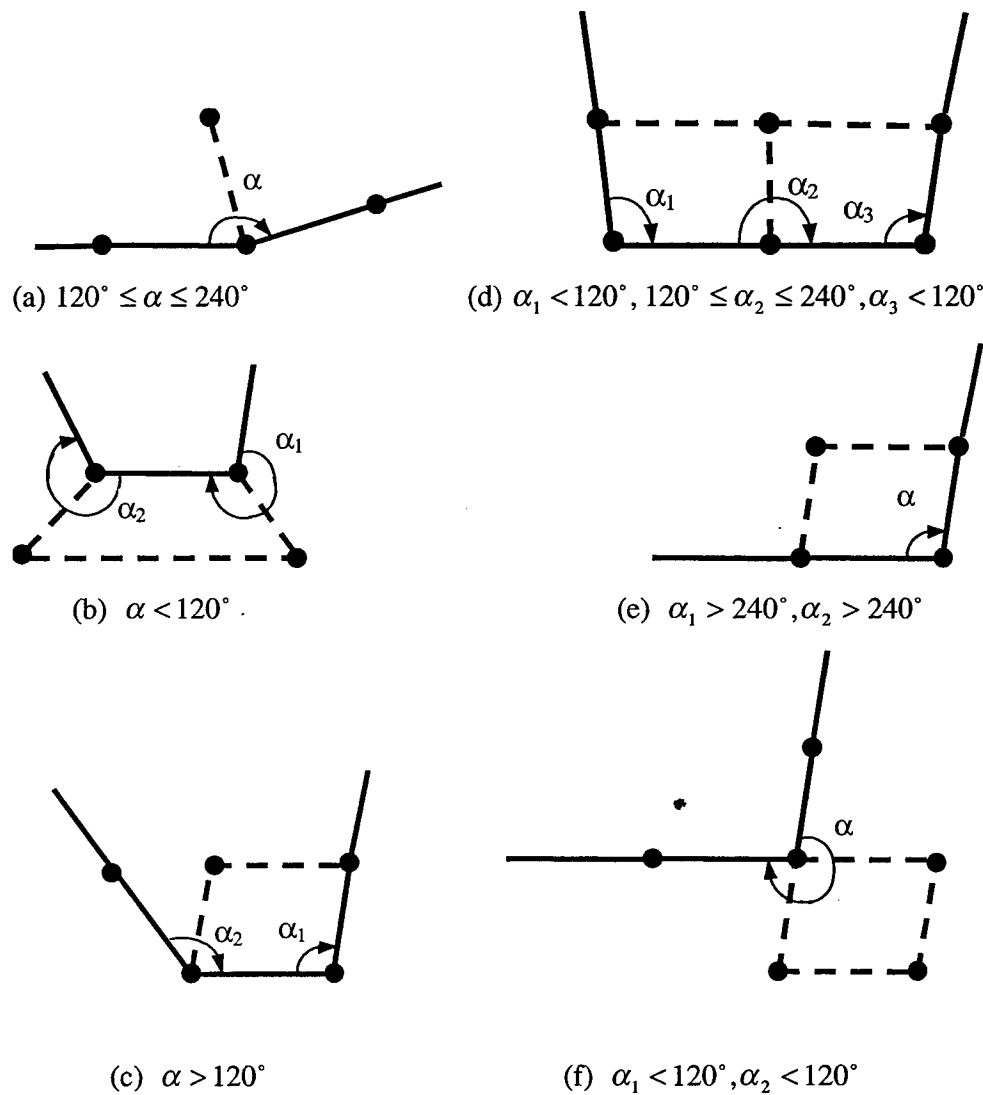


Figure 3-4 Offset node generation method

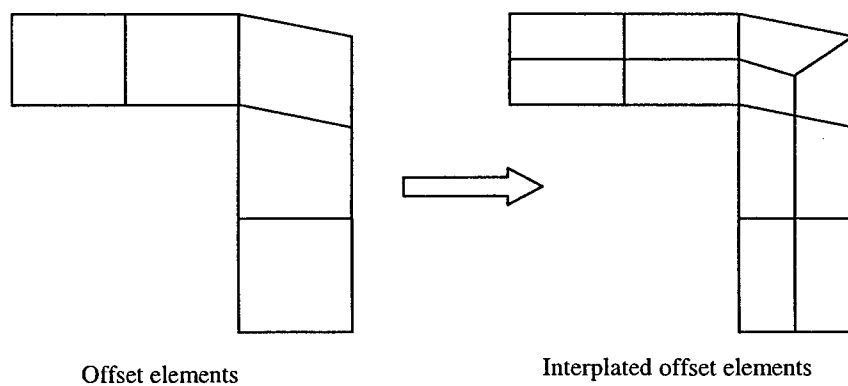


Figure 3-5 Interpolating the offset elements

3.2.3 Improvement of the distorted elements

Theoretically, the automatic mesh generation algorithm mentioned above can avoid the distorted elements by mesh smoothing if enough refined element sizes are prescribed on the boundary of structure. However, it also means that a large number of nodes are generated and follows a much longer calculating time. To overcome this drawback, we present a mesh improvement scheme.

As shown in Figure 3-6, there is an element with one of its interior angle ($>150^\circ$) being much larger than other three interior angles after mesh smoothing, which is unacceptable for finite element analysis. We can add one more node on its longer side (not including two sides forming the larger interior angle). Next, this element and its adjacent elements are refined into three elements. Then the mesh is smoothed again. Repeating this procedure for 2-3 times can eliminate the distorted elements. Figure 3-7 gives an example for this improvement with one time of modification.

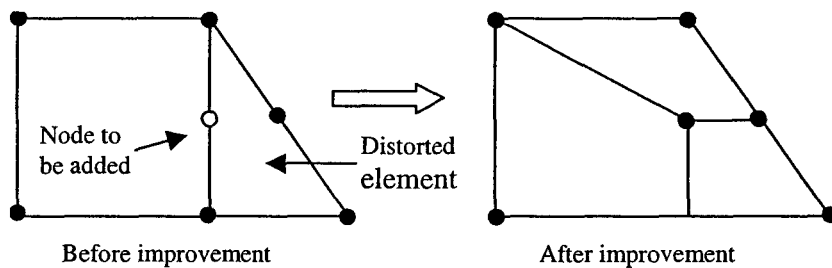


Figure 3-6 Improvement of the distorted elements

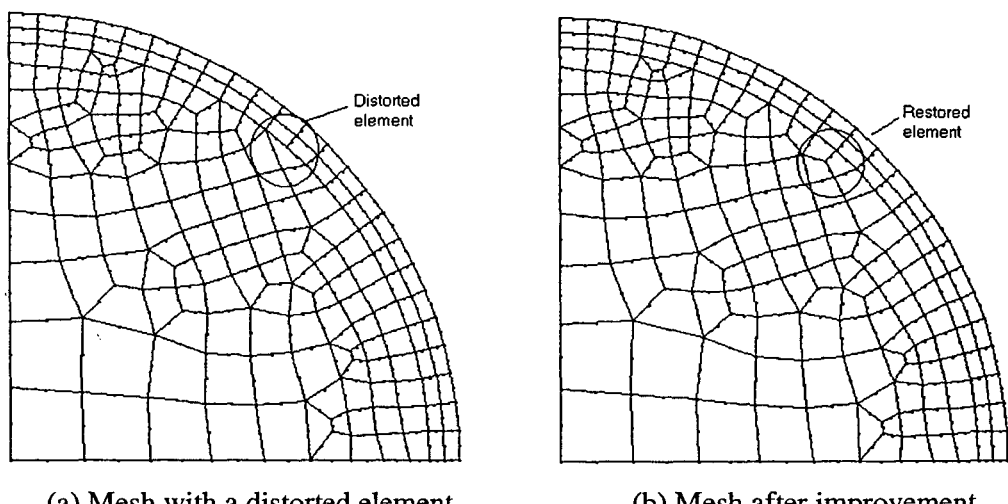


Figure 3-7 Mesh improvement

3.2.4 Mesh scheme

Based on the two-dimensional automatic mesh generation method described above, we can subdivide the cylindrical surface and the bonded patch by mapping them into a flat plane. First, two layers of offset elements are generated in the bonded patch along its boundary. Two more layers of offset elements are also subdivided outside adjacent to the boundary of the patch. Then the structure is divided into two continuous close loops, one is in the region of patch, and another is in the remained region. For each loop, the automatic mesh generator is applied to obtain quadrilateral elements. Then mesh is mapped back to the cylindrical coordinate system. To avoid long and narrow shape of the continuous loop, which makes the mesher perform badly [11], the loop of the shell is divided into two loops, as shown in Figure 3-8. A typical mesh generated by the presented scheme is shown in Figure 3-9.

It should be pointed out that the resulting bandwidth for a final mesh is very poor. So the nodes in the region of the bonded patch and remained region are renumbered according to its distance to the central point of the structure, respectively.

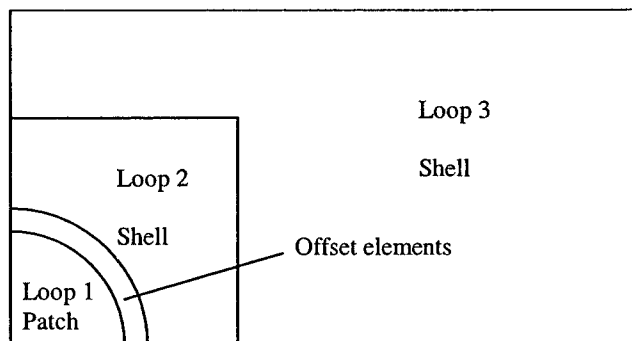
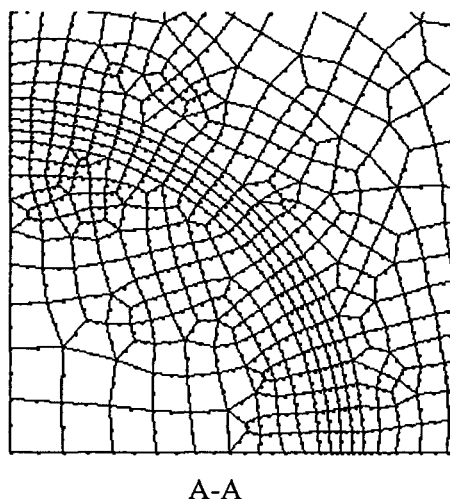
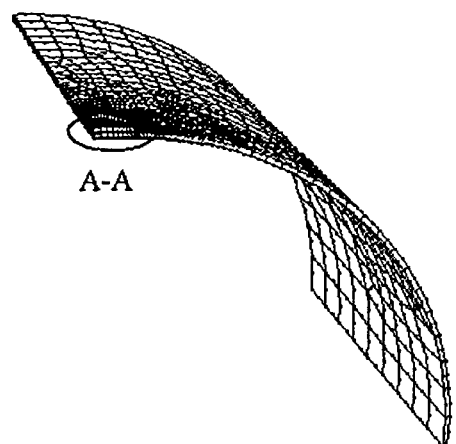
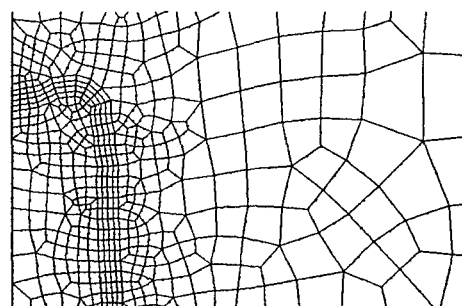
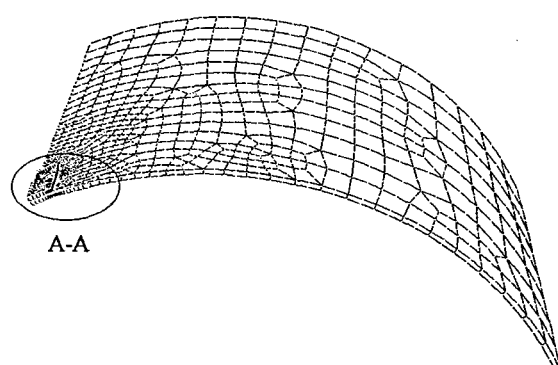


Figure 3-8 Mesh zoning scheme



(a) Mesh for circular patch



(b) Mesh for an optimum patch

Figure 3-9 Typical mesh used in current analysis

3.3 Shape optimization scheme

Based on the theoretical description in the above three sections, the shape optimization scheme is proposed as follows

- (1) Initialization. Input the structural data, material properties, mesh generation information (such as element size on the boundary, element size gradient, refinement coefficient, etc.), move limits.
- (2) Generate mesh and conduct stress analysis to obtain the stresses on the boundary of the bonded patch.
- (3) Sensitivity analysis. Move all the shape design variables from x_i to $x_i + \Delta x_i$ to obtain all the linearised coefficients used in SLP.
- (4) Check the current move limits. If the current limits are small enough, the new maximum stress is equal to that in the last iteration step and go to step (8).
- (5) Conduct linear programming analysis to find a feasible solution based on the current move limits. If no feasible solution is found, the new maximum stress is equal to that in the last iteration step and go to step (8).
- (6) Move the boundary of the bonded patch to the new shape.
- (7) Generate mesh using the new shape of the patch and conduct stress analysis to obtain the stresses on the boundary of the bonded patch.
- (8) Check the maximum stress. If the new maximum stress is larger than that in the last iteration step, reduce the move limits and go to step (4). If the new maximum stress is smaller than that in the last iteration step, go to step (3). If the new maximum stress is very close to that in the last iteration step, the shape optimization is converged and the program is stopped.

A software called BPATCH-Optimizer has been developed and verified through a number of examples.

3.4 Numerical examples and discussion

As shown in Figure 3-10, two circular patches with radius $r=15\text{mm}$ are externally bonded to a cylindrical shell. These two patches are located at the middle of the cylinder and only 1/8 of structure is considered due to its structural symmetry. The overall length of the shell is $W=300\text{mm}$. The external radius of the cylindrical shell is $R=150\text{mm}$. The thickness of both the cylindrical shell and the patches are all 2.0mm . The thickness of adhesive layer is $t=0.15\text{mm}$. An internal pressure $p=1.0\text{MPa}$ is applied to the cylindrical shell.

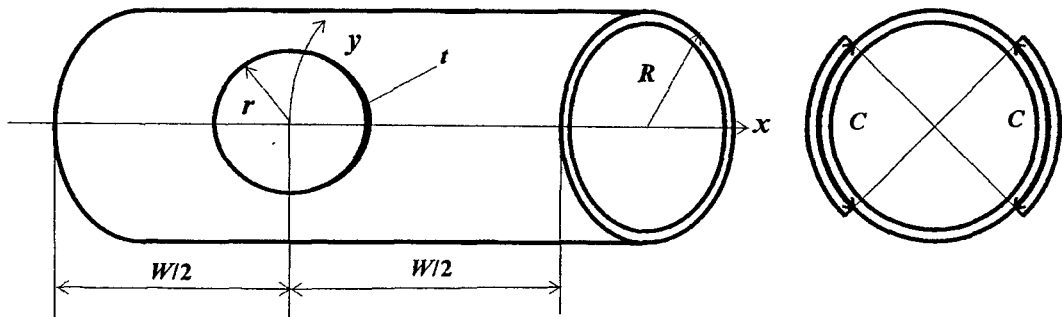


Figure 3-10 A cylindrical shell bonded to two circular patches on its external surface

The shell and the patch are assumed to be metallic with Young's modulus of $E=70\text{GPa}$ and Poisson's ratio of $\nu=0.3$. The adhesive used has a Young's modulus of $E_c=2.4\text{GPa}$ and a Poisson's ratio of $\nu_c=0.33$.

Both ends of the cylindrical shells are supported by rigid diaphragms, which allow displacements only in x -direction of the shell. The area of the bonded patch is limited between $3.0r^2$ and $6.0r^2$. A $1.2r \times 1.2r$ rectangle domain in the center of patch is defined as the basic domain. The move limit $d=0.35\text{mm}$ is used according to numerical test.

3.4.1. Shape evolution in the optimization process

Figure 3-11 depicts the shape evolution in the whole optimization process. The objective function is the maximum Von Mises stress evaluated on the node. To be clear, only a few selected optimization steps are plotted here. The final optimum shape step is 33.

It can be seen that the length of the bonded patch in y -direction keeps decreasing for all the shape evolutions. This is because the peak values of peel and shear adhesive stresses increase with the circumferential length of the patch, which can be verified by analyzing the rectangular patch with different circumferential length. The results show that the circumferential length of the bonded patch is the most important shape parameter to the adhesive stress for the investigated structure subjected to an internal pressure. From Figure 3-11, we can see that the circumferential length of the optimum patch is close to $0.6r$ for one quarter of the patch. This means that the total circumferential length of the optimum patch is $1.2r$ and it is coincide with the size of the prescribed basic domain. Therefore, it is predictable that the circumferential length of the bonded patch may become shorter if a smaller basic domain is given.

On the other hand, the length of the bonded patch in x -direction becomes shorter at first and then longer. According to the analysis of rectangular patch with different axial length, the axial length can slightly affect the peak value of the adhesive peel and shear stresses. Obviously, the effect of the axial length on the adhesive stresses changes with the circumferential length.

Table 3-2 gives the maximum adhesive stresses for different shape of patch. Comparing the first three rows, it can be found that the corner cut-off cannot decrease the peak adhesive stresses. In contrast, the peak adhesive stresses increase very much with the larger corner cut-off. Furthermore, the optimum shape of the bonded patch in Figure 3-11 shows that the corner should be moved outward instead of inward.

Comparing the patch shapes in step 5 and 10 in Figure 3-11, the presented optimization method can adaptively move the shape of the patch from a bad one (step 5) to a good one (step 10). In the final several steps, the move of shape design variables is smaller than that in other steps. Then the shape change is much smaller than that in other steps, which can be seen from step 25 to the final step (8 steps). This shows that the present optimization method can precisely evolve into the optimum shape. Therefore, the present method is suitable for shape optimization of a patch bonded to a curved surface.

3.4.2. Stresses on the node and Gaussian point

Two optimum shapes of the bonded patch, based on the stress on the node and Gaussian point respectively, are shown in Figure 3-12. The objective function is the maximum Von Mises stress. The optimum maximum adhesive stresses are given in Table 3-3. It can be found that stresses on the node and Gaussian point result in the similar optimum shapes. The Gaussian point is just close to the boundary of the patch. So the stresses on the Gaussian point cannot provide us enough accurate degree of stress concentration on the boundary of the adhesive layer. Consequently, the optimum stresses obtained from the Gaussian stress are slightly higher than those from the nodal stress (see Table 3-3). Therefore, all the other results discussed in the following are obtained according to the nodal stress.

3.4.3. Different objective functions

In Section 3.1.3, we presented three different objective functions, which are the maximum peel stress, the maximum shear stress and the maximum Von Mises stress. The purpose to define the objective function in this way is to allow consideration of different possible failure modes of adhesive layer.

Figure 3-13 depicts the optimum shapes of the bonded patch by minimizing different maximum adhesive stresses. The peak adhesive stresses obtained from these optimum shapes are given in Table 3-2. It should be pointed out that the optimum shape of the bonded patch obtained from the maximum Von Mises stress as the objective function is used as the initial shape of the bonded when we conduct other two analysis. It is clearly shown in Figure 3-13 that the optimum shapes for different objective functions are similar to each other. Therefore, it may not be necessary to conduct several optimization analyses to find an optimum shape of the bonded patch to cover all the possible failure modes. Certainly, we must determine which stress is the key parameter to the strength of the adhesive layer.

From Table 3-2, we can see that the peak stresses in the adhesive layer can be reduced dramatically by optimizing the geometrical shape of the bonded patch. Especially for the peel stress, it can be reduced in a large amount up to 58.8% in this example. In fact, the peel stress

is closely related to the circumferential length of the bonded patch. For the limitation of the basic domain, the circumferential length of the patch attains the value as per the basic domain. The peel stress should be reduced further if a smaller basic domain is given. The shear stress and Von Mises stress are reduced by 24.3% and 29.0%, respectively. This shows that the shape optimization can efficiently reduce the peak value of adhesive stresses. The objective function should be chosen according to the failure mode in its application.

3.4.4. Effect of curvature

Figure 3-14 gives the optimum shapes of the bonded patch for different radius of the cylindrical shell with the maximum Von Mises adhesive stress as the objective function. The optimum adhesive stresses are given in Table 3-4. It can be seen that all the optimum shapes have almost same shape in the circumferential direction. The length of the patch in the longitudinal direction increases with the radius of the cylindrical shell. This is because the length of the patch in the circumferential direction controls the maximum adhesive stress in this circumstance. Using as shorter circular length of the patch as possible can improve the strength of the adhesive layer.

3.4.5 Composite patch

A composite patch bonded to a cylindrical surface is investigated by the present optimization method. The composite material is assumed to have following properties

$$\begin{aligned} E_1 &= 181.0 \text{ GPa} & E_2 = E_3 &= 10.3 \text{ GPa} & G_{12} = G_{13} &= 7.17 \text{ GPa} \\ G_{23} &= 4.02 \text{ GPa} & \mu_{12} = \mu_{13} &= 0.28 & \mu_{23} &= 0.28 \end{aligned}$$

Two kinds of stacking sequences are analyzed, which are $[0_2/90_2/0_2/90_2]_s$, $[90_2/0_2/90_2/0_2]_s$. The thickness of each single ply is 0.127mm. Because of the cross-ply stacking, we can use the same mesh scheme as metal patch in the analysis.

Figure 3-15 depicts the optimum shape of the composite patch. The objective function is the maximum Von Mises adhesive stress. The stresses for circular patch and optimum patch are

given in Table 3-5. It can be seen that there isn't much difference of the optimum shape for two kinds composite patch. Furthermore, they are similar to the optimum shape obtained from the metal patch. This is because the composite patch used here is a quasi-isotropic laminate.

Although similar optimum shapes are obtained for these two composite patches, the peel stresses in the adhesive layer are very different. As shown in Table 3-5, the peel stress of $[90_2/0_2/90_2/0_2]_s$ patch is much smaller than that of $[0_2/90_2/0_2/90_2]_s$ patch for both optimum and circular patches. This is believed to be mainly caused by the mismatch of stiffness in the circumferential direction between the adhesive layer and lower surface ply of the bonded patch. For the load case considered here, the patch is subjected to a high stress in the circumferential direction [6]. For $[90_2/0_2/90_2/0_2]_s$, the first ply adjacent to the adhesive layer is 90° , which is in the circumferential direction. The 90° surface ply is less stiff than the aluminum parent shell in the circumferential direction, thus results in a low peel stress. In contrast, the peel stress for $[90_2/0_2/90_2/0_2]_s$ patch is higher than that for $[0_2/90_2/0_2/90_2]_s$ patch due to the fact that the 0° surface ply is much stiffer than the aluminum parent shell.

The results in Table 3-5 also show that the optimum shape of patch can decrease the stress in the adhesive layer significantly.

3.4.6. Optimization based on thermal stress

To reduce the thermal residual stress cased by temperature change during the bonding process, shape optimization based on thermal stress is performed here. All the geometrical sizes of the structure are as same as those described at the beginning of this section, together with the same material of cylindrical shell and adhesive layer. The patch is a composite one with the same material prosperities as those in Section 3.4.5. The stacking sequence is $[90_2/0_2/90_2/0_2]_s$.

The coefficient of thermal expansion of the metallic shell is assumed to be $\alpha = 0.24 \times 10^{-4}$. The coefficients of thermal expansion of the composite patch are taken as $\alpha_1 = 0.63 \times 10^{-7}$, $\alpha_2 = 0.288 \times 10^{-4}$, in which subscript 1 indicates the fiber direction and subscript 2 the transverse direction. It should be pointed out that the thermal effect of the adhesive layer is not considered here.

The applied thermal load is a temperature change from 220°C down to 20°C. The boundary condition is the same as above.

Figure 3-16 depicts the similar optimum shape of the composite patch. However, the adhesive stress remains very high. Table 3-6 gives the adhesive stresses before and after shape optimization. The maximum Von Mises stress is reduced by 24.2%. However, the maximum peel stress is increased by 5.7%.

3.4.7. Different boundary support

All the examples above have same boundary support. To investigate the boundary effect on the optimum shape of patch, the both ends of cylindrical shell are fixed. Two kinds of patches are considered, which are metallic and composite patches. The stacking sequence of composite patch is [90₂/0₂/90₂/0₂]_s. All other parameters are the same as described above.

Figure 3-17 depicts the shape evolution of metallic patch boned to a cylindrical shell with the maximum Von Mises stress as the objective function. A total of 19 steps of shape change were required to obtain the optimum shape. Obviously, the circumferential length of patch for the optimum shape is much longer than that in Figure 3-11. The width of the patch for the optimum shape in the longitudinal direction remains not significantly changed from the radius of the initial shape. This shows that the axial constraint can dramatically affect the optimum shape. It is believed that the internal pressure and the fixed end constraints create membrane stress in the longitudinal direction, which in turn yields high peel stress along the longitudinal boundary of the patch. The created high peel stress restrains outward boundary movement in the longitudinal direction.

Figure 3-18 shows two optimum shapes of metallic patch with the objective function being the maximum peel stress and the maximum Von Mises stress, respectively. The two optimum shapes almost coincide to each other.

Figure 3-19 and 3-20 depict the shape evolution and optimum shapes for the composite patch. Comparing the optimum shapes with those in Figure 3-15, the difference is similar to that observed for the cases of metallic patch. However, it should be pointed out that the optimum patches evolved based on different objective functions, i.e., the maximum peel stress and the maximum Von Mises stress, are quite different, although their shapes are similar.

Table 3-7 gives the optimum maximum stress in adhesive layer for metallic and composite patch bonded to cylindrical shell with fixed boundary support. Comparing these results with those obtained previously, we can find that the maximum Von Mises stress changes slightly. However, for the composite patch with the maximum peel stress being the objective function, the optimum maximum peel stress decreases significantly, up to 57.0%. For the case with the maximum Von Mises stress being the objective function, the maximum peel stress remains very high. Thus it is appropriate to choose the maximum peel stress as the objective function in this circumstance if the maximum peel stress causes adhesive failure.

Table 3-2 The maximum adhesive stresses with different shapes of the boned patch
(The radius of the cylindrical shell = 150mm)

Shape of the bonded patch		Peel stress (MPa)	Shear stress (MPa)	Von Mises stress (MPa)	$(\sigma_0 - \sigma_a)/\sigma_0$ **
Square		14.22 (14.00,15.00)*	18.12 (14.00,15.00)	19.90 (14.00,15.00)	
Square with corner cut-off		13.89 (8.57, 14.92)	18.96 (9.61, 14.70)	20.45 (8.57, 14.92)	
Circle		16.38 (0.00,15.00)	19.66 (0.00,15.00)	21.82 (0.00,15.00)	
Optimum	Objective: Peel	6.75 (19.90, 8.42)	15.40 (19.90, 8.42)	15.74 (19.90, 8.42)	58.8%
	Objective: Shear	6.90 (18.90, 8.40)	14.88 (18.90, 8.40)	15.58 (18.90, 8.40)	24.3%
	Objective: Von Mises	7.81 (13.98, 9.09)	14.99 (13.98, 9.09)	15.49 (13.98, 9.09)	29.0%

*The values in the brace are the nodal coordinate where the maximum stress is located.

** σ_a is the value of objective function and σ_0 is the corresponding value of the circular patch.

Table 3-3 The optimum maximum adhesive stress based on nodal and Gaussian stresses
(The radius of the cylindrical shell = 150mm)

Objective function	Nodal stress (MPa)	Gaussian Stress (MPa)
Peel stress	7.81 (13.98, 9.09)*	8.42 (0.00, 10.32)
Shear stress	14.99 (13.98, 9.09)	15.57 (0.00, 10.32)
Von Mises Stress	15.49 (13.98, 9.09)	16.31 (0.00, 10.32)

* The values in the brace are the nodal coordinate where the maximum stress is located.

Table 3-4 The optimum maximum adhesive stresses for different radius of cylindrical shell

Radius of Shell (mm)	Peel stress (MPa)	Shear stress (MPa)	Von Mises stress (MPa)
150	16.38 (7.81)*	19.66 (14.99)	21.82 (15.49)
200	21.45 (9.84)	26.11 (20.24)	28.90 (20.91)
250	26.59 (12.27)	32.60 (25.23)	36.03 (26.70)
300	31.61 (15.17)	39.02 (30.69)	43.08 (31.35)

* The values in the brace are the corresponding maximum stress for the optimum patch with initial shape of patch being circle.

Table 3-5 The optimum maximum adhesive stresses for composite patch (Objective function:

Maximum Von Mises stress on node. The radius of the cylindrical shell = 150mm)

Stacking sequence	Patch shape	Maximum Peel stress	Maximum Shear stress	Maximum Von Mises stress	$(\sigma_0 - \sigma_a)/\sigma_0$ **
$[90_2/0_2/90_2/0_2]_s$	Circle	12.91 (0.00,15.00)*	21.83 (0.00,15.00)	23.07 (0.00,15.00)	24.1%
	Optimum	3.72 (0.0, 9.39)	17.40 (13.98,9.00)	17.51 (13.98,9.00)	
$[0_2/90_2/0_2/90_2]_s$	Circle	18.52 (0.00,15.00)	20.42 (0.00,15.00)	23.05 (0.00,15.00)	28.2%
	Optimum	8.79 (2.99, 9.31)	15.78 (13.97,9.00)	16.54 (13.97,9.00)	

*The values in the brace are the nodal coordinate where the maximum stress is located.

** σ_a is the value of objective function and σ_0 is the corresponding value of the circular patch.

Table 3-6 The optimum maximum adhesive stresses for composite patch (Objective function: Maximum Von Mises stress on node. The radius of the cylindrical shell = 150mm)

Patch shape	Maximum Peel stress (MPa)	Maximum Shear stress (MPa)	Maximum Von Mises stress (MPa)	$(\sigma_0 - \sigma_a)/\sigma_0$ **
Circle	135.27 (14.97, 0.98)*	231.58 (0.00, 15.00)	244.42 (0.00, 15.00)	24.2%
	142.99 (21.36, 5.89)	184.09 (14.00, 9.00)	185.37 (14.00, 9.00)	

*The values in the brace are the nodal coordinate where the maximum stress is located.

** σ_a is the value of objective function and σ_0 is the corresponding value of the circular patch.

Table 3-7 The optimum maximum adhesive stresses for the fixed end of cylindrical shell bonded metallic or composite patch (The radius of the cylindrical shell = 150mm)

Lay-up	Shape of the bonded patch	Peel stress (MPa)	Shear stress (MPa)	Von Mises stress (MPa)	$(\sigma_0 - \sigma_a)/\sigma_0$ **
Metallic patch	Circle	13.06 (0.00, 15.00)	17.93 (0.98, 14.97)	19.42 (0.00, 15.00)	40.7%
		7.75 (0.00, 12.66)	15.35 (0.00, 12.66)	16.02 (0.00, 12.66)	
	Optimum	7.89 (0.00, 12.66)	15.32 (0.00, 12.66)	15.99 (0.00, 12.66)	17.7%
		9.94 (0.00, 15.00)	19.28 (0.00, 15.00)	20.11 (0.00, 15.00)	
Composite patch	Circle	4.27 (9.85, 11.14)	16.89 (8.86, 11.29)	17.09 (8.86, 11.29)	57.0%
		7.09 (12.89, 1124)	16.82 (0.00, 12.75)	17.07 (0.00, 12.75)	
	Optimum	4.27 (9.85, 11.14)	16.89 (8.86, 11.29)	17.09 (8.86, 11.29)	15.1%
		7.09 (12.89, 1124)	16.82 (0.00, 12.75)	17.07 (0.00, 12.75)	

*The values in the brace are the nodal coordinate where the maximum stress is located.

** σ_a is the value of objective function and σ_0 is the corresponding value of the circular patch.

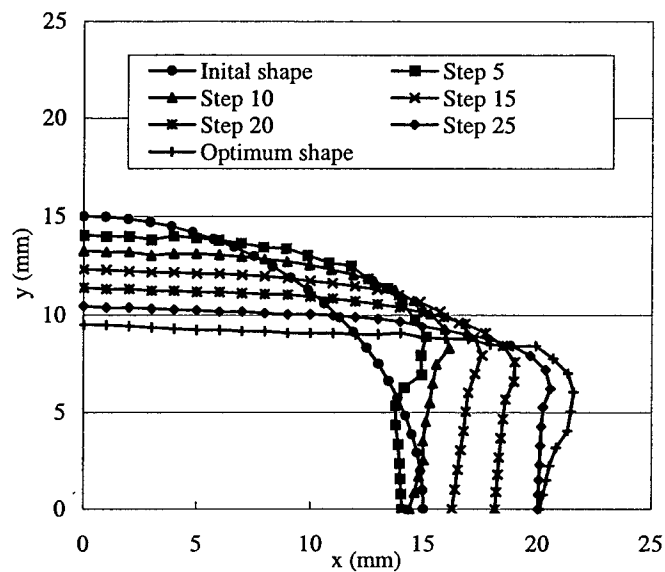


Figure 3-11 Shape evaluation in the optimization process
(The objective function is nodal Von-Mises stress)

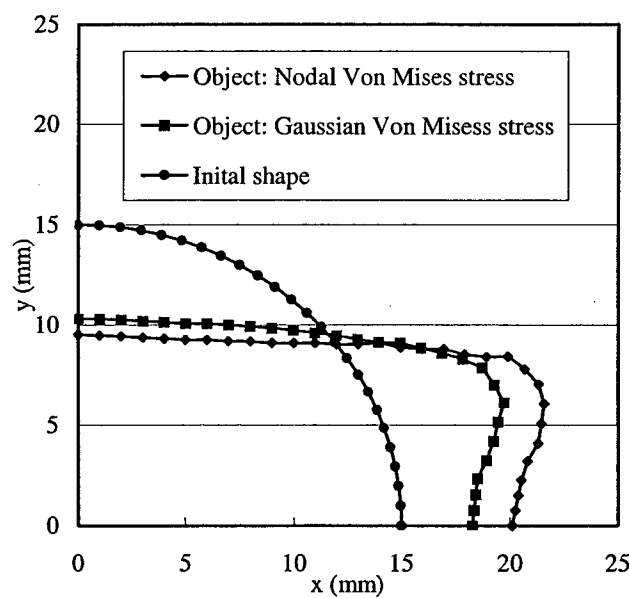


Figure 3-12 Optimum shape based on Gaussian and nodal stress
(The objective function is Von-Mises stress)

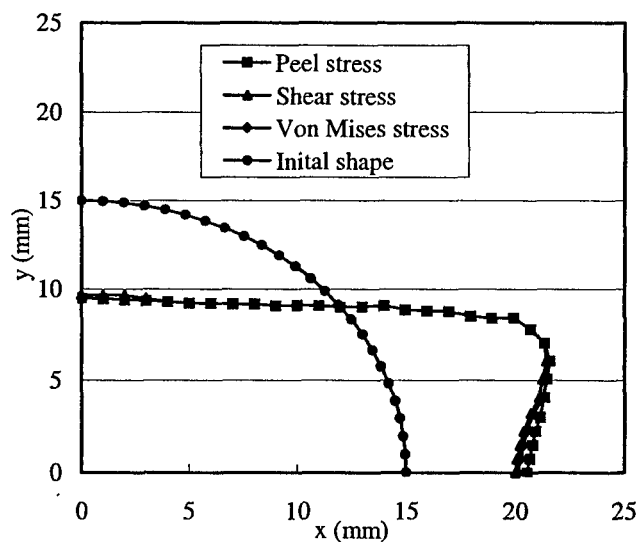


Figure 3-13 Optimum shape of patch based on different objective functions

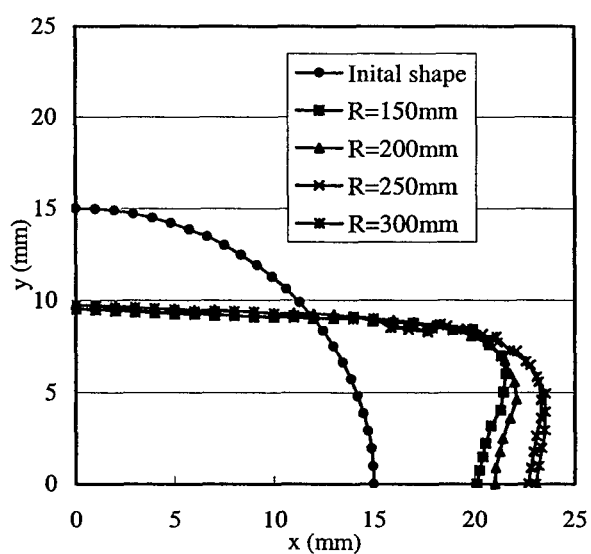


Figure 3-14 Optimum shape of patch bonded to shell with different curvature

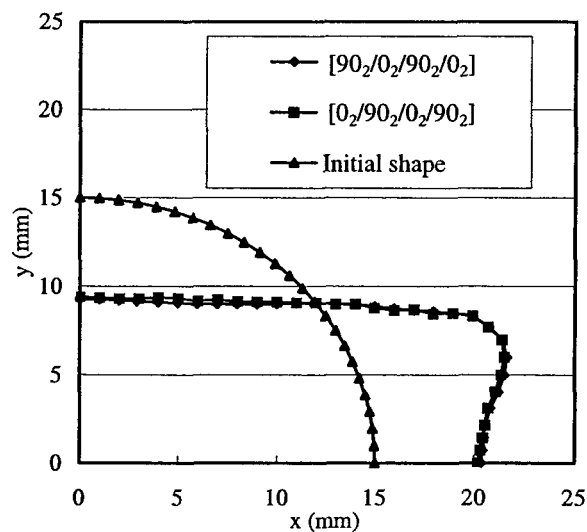


Figure 3-15 Optimum shape of composite patch with different stacking sequence

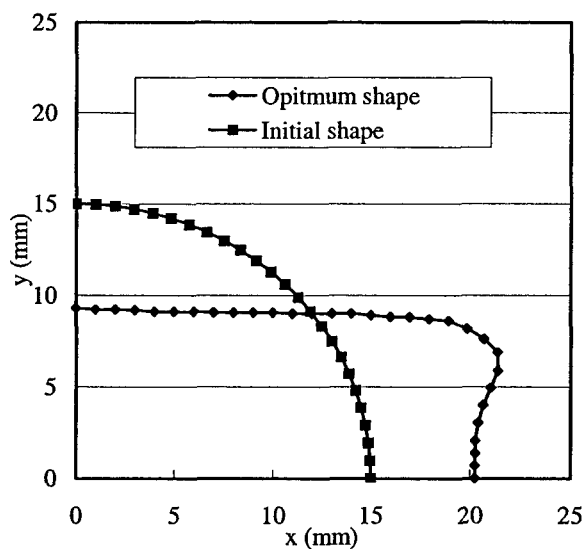


Figure 3-16 Optimum shape of composite patch subjected to temperature change

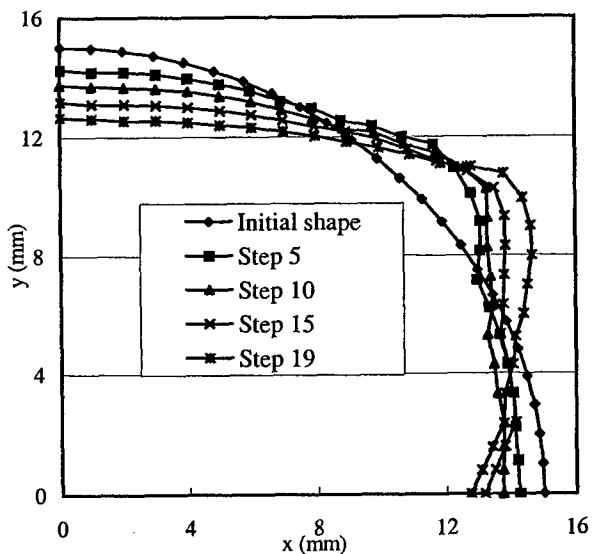


Figure 3-17 Shape evolution for the fixed end of cylindrical shell bonded metallic patch

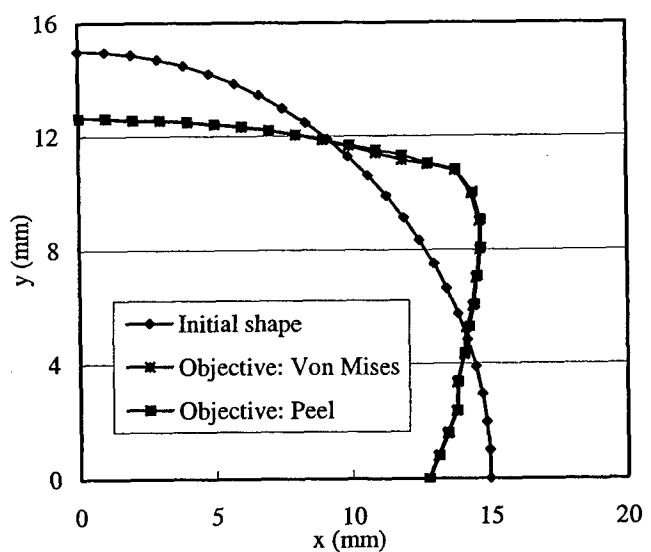


Figure 3-18 Optimum shape based on different objective functions for the fixed end of cylindrical shell bonded metallic patch

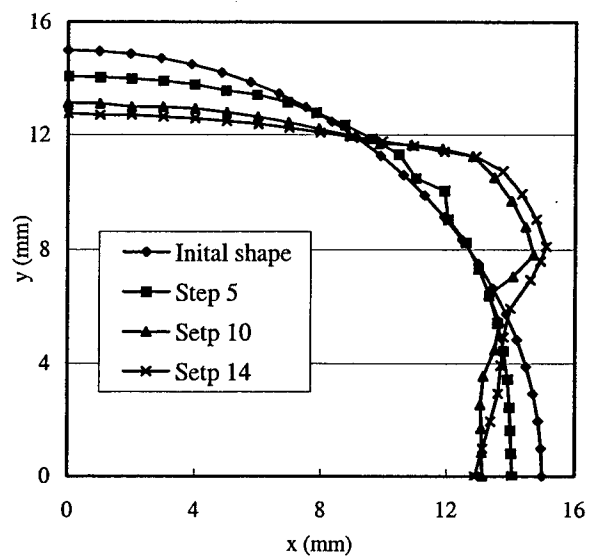


Figure 3-19 Shape evolution for the fixed end of cylindrical shell bonded composite patch

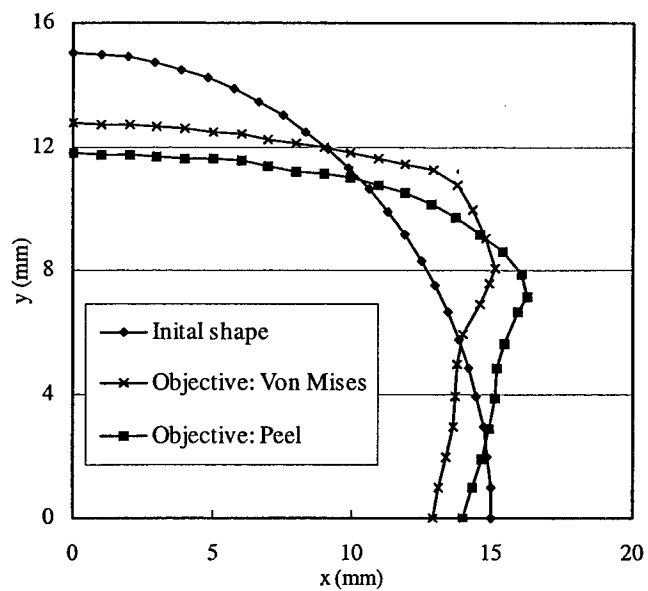


Figure 3-20 Optimum shape based on different objective functions for the fixed end of cylindrical shell bonded composite patch

4. Optimization of the ply drop-offs of composite patch

The stress concentration, which occurs in the adhesive layer along the periphery of the bonded patch, can dramatically reduce the bonding strength. It is thus desirable to minimize the adhesive stresses by optimizing the shape of the curved bonded patch. However, even for the optimum shape of the patch, the stress concentration near the boundary of the adhesive layer, which is caused by the discontinuities of material and geometry on the bonding interface, can still be high too. Therefore, it is necessary to relieve the stress concentration on the boundary of the adhesive layer by employing other techniques.

There are two methods available to improve the stress concentration on the interface between the different materials. From the analysis of the bi-material connection, it was found that the stress singularity might disappear by choosing appropriate combinations of material constants in the two materials when the geometry is fixed [13, 14]. In the second method, changing the geometric shapes, such as tapering, along the periphery of the bonding interface can also reduce the stress concentration, according to the research results for flat adhesive joints [6, 15].

In general, the material and the geometry of the curved surface are pre-determined before we start to optimally design the bonded patch. Then only the material and geometry of the bonded patch can be selected as design variables. This makes it extremely difficult to choose an adequate combination of material constants for the bonded patch because the materials available are in general limited. Composite material provides us more opportunities to design the properties of material by designing its lay-up. This method will be discussed in the next section. In this section, we focus on optimum design of the geometry of the bonding interface in the through thickness direction, i.e., optimum tapering.

Based on the current knowledge of steel wedging and flat bonding design, the wedge angle in the both adherents is a key geometric parameter for the alleviation or even disappearance of stress concentration. The stress concentration can even be removed by cutting the adherent at an appropriate wedge angle on its boundary. Moreover, a wedge angle is very easy to implement for composite patch by the ply drop-off. Therefore, the wedge or tapering angle is selected as the optimization parameter.

The wedge angle is suitable for flat joint or repair design because its cutting plane is a flat one. This cutting plane becomes a curved one if the wedge is applied to a curved joint design. For the sake of convenience, we use a similar parameter, the drop-off width, to replace the wedge angle, which is described in the following sections.

In this section, a detailed stress analysis method of the bonded composite patch with the ply drop-offs is presented first. Then a mesh scheme for the ply drop-off is given to conduct the stress analysis. It should be noted that the ply drop-off in the current analysis is limited to be uniform to reduce the computational time. As a matter of fact, the present method can also be applied to conduct an analysis of the non-uniform ply drop-off. Finally, the effects of ply drop-off on the adhesive stresses for the different shape of patch are investigated.

4.1. Definition of the ply drop-off width

Figure 4-1 depicts a curved composite patch with the ply drop-off is bonded to a curved surface. The ply drop-off takes place on the all the boundary of every ply of the bonded patch. The definition of the wedge angle and the cutting plane are shown in Figure 4-2. It can be clearly seen that the wedge angle can fully describe the ply drop-offs for a flat bonded patch (see Figure 4-2(a)). Accordingly, when the geometry of flat is projected to a curved plane, (as shown in Figure 4-2(b)), the flat cutting plane becomes a curved one. Then the wedge angle is unsuitable to define the ply drop-offs for the curved patch. Therefore, the drop-off width d is introduced to define how every ply is dropped off (see Figure 4-2(b)).

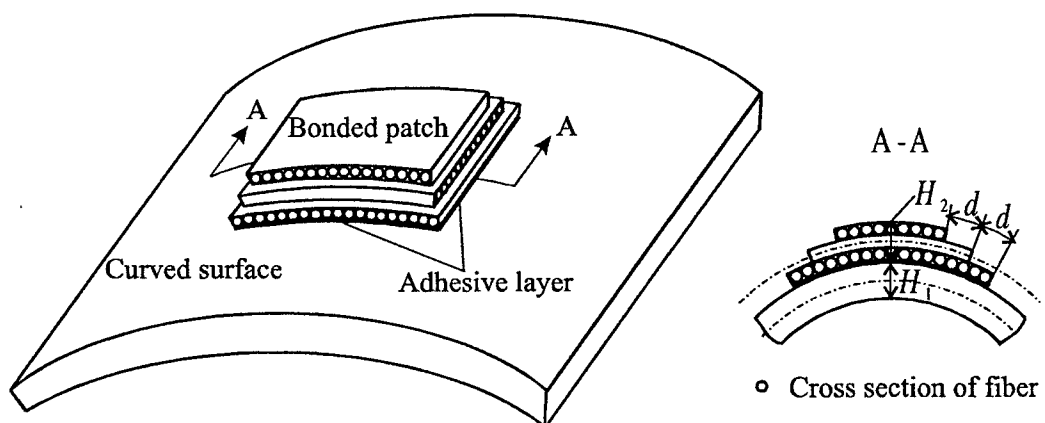


Figure 4-1 A composite patch with the ply drop-offs is bonded to a curved surface

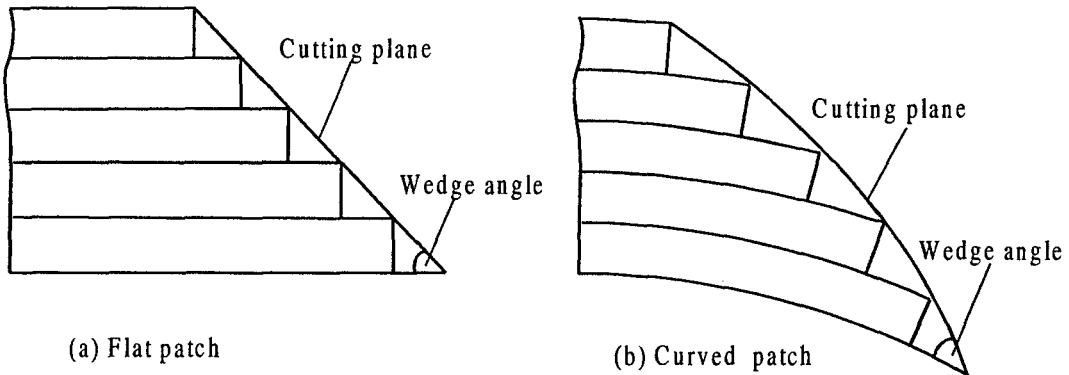


Figure 4-2 The wedge angle and cutting plane of patch with the ply drop-offs

4.1.1 Ply drop-off scheme for special shape of patch

For some special shapes of patch, such as a circular or square patch, we can define the drop-off width as the normal distance from the boundary of one ply to that of adjacent ply. It means that the drop-off width keeps uniform along all the boundary of the bonded patch. Moreover, the drop-off region can be extended to its central point, which enable us design a long enough total drop-off width from its external boundary to its central point. Figure 4-3 gives the definition of the ply drop-off for these two kinds of typical shape of patch.

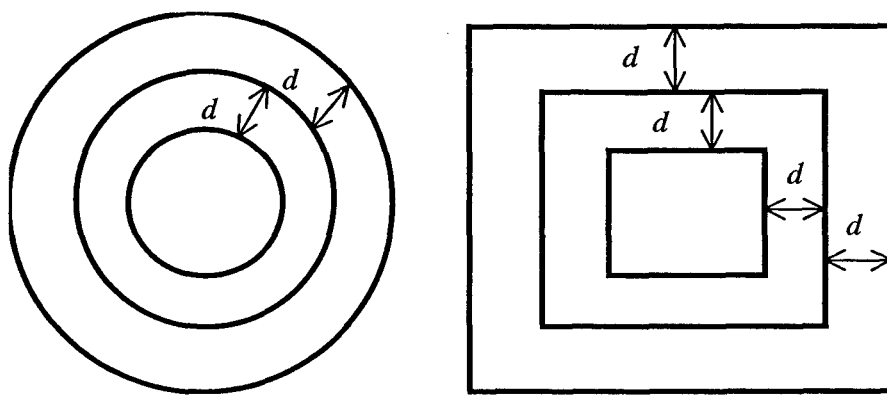


Figure 4-3 Definition of the ply drop-off width

4.1.2. Ply drop-off scheme for general shape of patch

Although it is easy to find the new boundary for a new ply drop-off for the shape of patch mentioned above by the definition of ply drop-off width in Section 4.1.1, it may fail to find such a new boundary for a new ply drop-off if an arbitrary shape of patch is given. For example, for the optimal shapes of the bonded patch, which are obtained from shape optimization, only a very small range of drop-off width can be applied to get the new boundary with uniform drop-off width. However, a longer drop-off width can reduce the highly concentrated adhesive stress on the boundary of the adhesive layer. Therefore, we need to design a scheme to calculate the new boundary for each ply drop-off.

In this report, we only consider the cylindrical surface bonded with a patch. Furthermore, we assume that the bonded patch is a symmetrical one, which has two symmetrical axes. Then the ply drop-off width is defined as the distance between two boundaries on its symmetrical axes, as shown in Figure 4-4. To be convenient, we can calculate the new boundary of the drop-off in a flat plane. In Figure 4-4, x and y are the two symmetrical axes of the bonded patch, with the length $2a$ and $2b$, respectively. The ply drop-off width d is defined on these two axes. Then the new boundary of the drop-off can be given by

$$\begin{aligned} x_1 &= x_0 \cdot \frac{a-d}{a} \\ y_1 &= y_0 \cdot \frac{b-d}{b} \end{aligned} \tag{4-1}$$

where x_0 , y_0 are the coordinate of the node on the initial boundary of patch. x_1 , y_1 are the coordinate of the node on the new drop-off boundary. It can be verified that the drop-off scheme described here can give the same drop-off shape as that obtained in Section 4.1.1 if the initial shape of the bonded patch is circular and square.

Figure 4-5 depicts an example of drop-off shape of the bonded patch obtained by the method presented above.

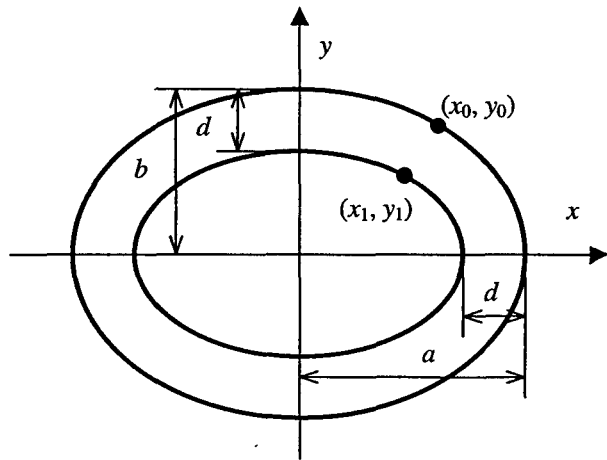


Figure 4-4 Ply drop-off definition for general shape of patch

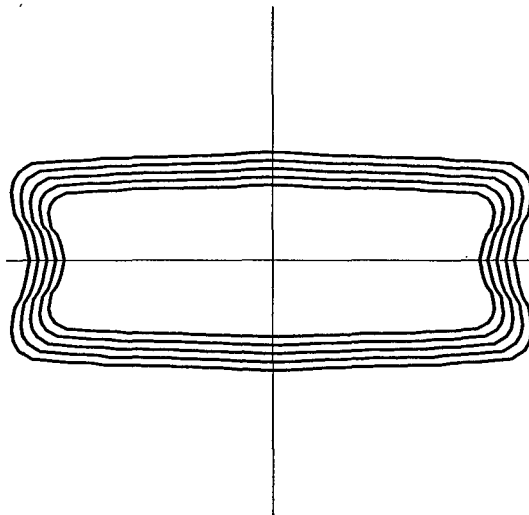


Figure 4-5 Ply drop-off of a general shape of patch (Projected into a flat plane)

4.1.3. Uniform ply drop-off width

It should be pointed out that it is possible to define different drop-off width between two different adjacent plies, which means that the cutting plane at the end of the patch is a curved one instead of a flat one even for a flat patch in Figure 4-2(a). However, to simplify the problem and reduce the computing time, a uniform drop-off width is assumed to the bonded composite patch. Then we can reduce the design parameter to a single uniform drop-off width, which can be found by employing an one-dimensional optimization method.

4.2. Structural analysis of the bonded composite patch with the ply drop-offs

For the shell element used here, all the nodal displacements in an element are referred to the mid-plane of the element and the thickness remains constant in the element. In the former analysis, the thickness of both the bonded patch and the curved surface are constant and the adjacent elements share the same nodes (defined in their mid-planes) in their joining plane. So all the nodal displacements are referred to the mid-plane of the bonded patch or the curved surface.

However, the existence of the ply drop-offs makes the thickness of the patch change with the ply drop-offs. This results in different mid-planes for any two adjacent shell elements along the ply drop-off direction because of both elements having different thickness. It follows that the nodes defined in the adjacent two elements along the ply drop-off direction are located at the different position in their joining normal, which results in two nodes in one normal. These two nodes should be reduced to one node according to the assumed displacement field. Then we can define a common reference plane, called master plane. The node in this master plane is called master node. Accordingly, the nodes defined in the adjacent elements are called slave node. The master node is used in the total stiffness matrix, which indicates that the total stiffness matrix is referred to the master plane. Before assembling the element stiffness matrix (referred to its own mid-plane) into the total stiffness matrix, the element stiffness matrix must be transformed from the slave node to the master node. It is worthy noting that the master node can be arbitrary selected in the joining normal.

In Figure 4-6, we define the node in the mid-plane of the bonded patch without the ply drop-offs as the master node, the node in mid-plane of the shell element as slave node. All the nodal displacements in the patch are referred to these master nodes. It is then convenient to transform all the nodal displacements from the mid-plane of an element to the corresponding master node.

According to the first order shear deformation theory for plate and shell, we have the relationship of the displacements between the slave node and the master node

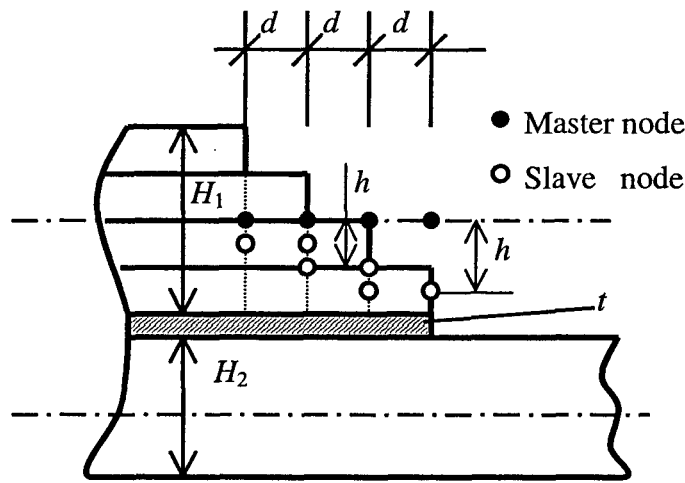


Figure 4-6 Master and slave nodes in the ply drop-offs

$$\begin{bmatrix} u_s \\ v_s \\ w_s \\ \theta_{xs} \\ \theta_{ys} \end{bmatrix} = \begin{bmatrix} 1 & 0 & 0 & 0 & -h \\ 0 & 1 & 0 & h & 0 \\ 0 & 0 & 1 & 0 & 0 \\ 0 & 0 & 0 & 1 & 0 \\ 0 & 0 & 0 & 0 & 1 \end{bmatrix} \begin{bmatrix} u_m \\ v_m \\ w_m \\ \theta_{xm} \\ \theta_{ym} \end{bmatrix} \quad (4-2)$$

where h is the distance between the corresponding pairs of slave and master nodes. The subscript 'm' denotes the displacements of the master node, and the subscript 's' means the displacements of the slave node.

Rewrite equation (4-2) in a vector form

$$\{q_s\} = [T]\{q_m\} \quad (4-3)$$

where $\{q_m\}$ is the nodal displacement vector referred to the master node, $\{q_s\}$ is the nodal displacement vector referred to the slave node.

Then all the element stiffness matrices are evaluated on their own mid-plane and all the nodal displacements are referred to the slave nodes. The strain energy in the element can be given by

$$U = \frac{1}{2} \int_A ([B] \{q_s\}^e)^T [D] [B] \{q_s\}^e dA \quad (4-4)$$

where $\{q_s\}^e$ is the nodal displacement vector in the element referred to the slave node. $[B]$ is the element geometrical matrix. $[D]$ is the elastic matrix referred to the mid-plane of the element. A is the area of the element.

Substituting equation (4-3) into equation (4-4), we have

$$U = \frac{1}{2} \int_A ([B] [T] \{q_m\}^e)^T [D] [B] [T] \{q_m\}^e dA \quad (4-5)$$

According to the variation theory, we can obtain the element stiffness matrix evaluated on the master node

$$\begin{aligned} [K_m]^e &= \int_A ([B] [T])^T [D] [B] [T] dA = \int_A [T]^T [B]^T [D] [B] [T] dA \\ &= [T]^T \left(\int_A [B]^T [D] [B] dA \right) [T] = [T]^T [K_s]^e [T] \end{aligned} \quad (4-6)$$

where $[K_m]^e$ is the element stiffness matrix evaluated on the master nodes and $[K_s]^e$ is the element stiffness matrix evaluated on the slave node.

Therefore, the element stiffness matrix is calculated in terms of the displacements referred to the mid-plane of element, i.e., the slave nodal displacements. Then the element stiffness matrix is transformed into that under master nodes by equation (4-6). Finally, the element stiffness matrix is assembled to the global stiffness matrix.

4.3. Mesh scheme

According to the structural analysis method described above, every ply drop-off must be divided into different elements. To improve the precision of stress analysis, sever similar

elements should be added before and after the ply drop-offs. Then the automatic mesh generator can be used to generate a mesh for the remaining part of the structure. Figure 4-7 depicts a mesh scheme of a square bonded patch with 4-layers of the uniform ply drop-offs. There is also one layer of similar elements adjacent to the ply drop-off region. In fact, there should be more layers of similar elements outside the ply drop-offs in the analysis. Figure 4-8, 4-9, 4-10 and 4-11 depict typical meshes generated by this mesh scheme.

The total number of node increases dramatically with the total number of ply of the composite patch because every ply drop-off must be divided into at least one element. To improve the computational efficiency, the structural parts that don't have ply drop-offs and are automatically meshed can be analyzed first as substructures, which can be incorporated into the ply drop-off zone.

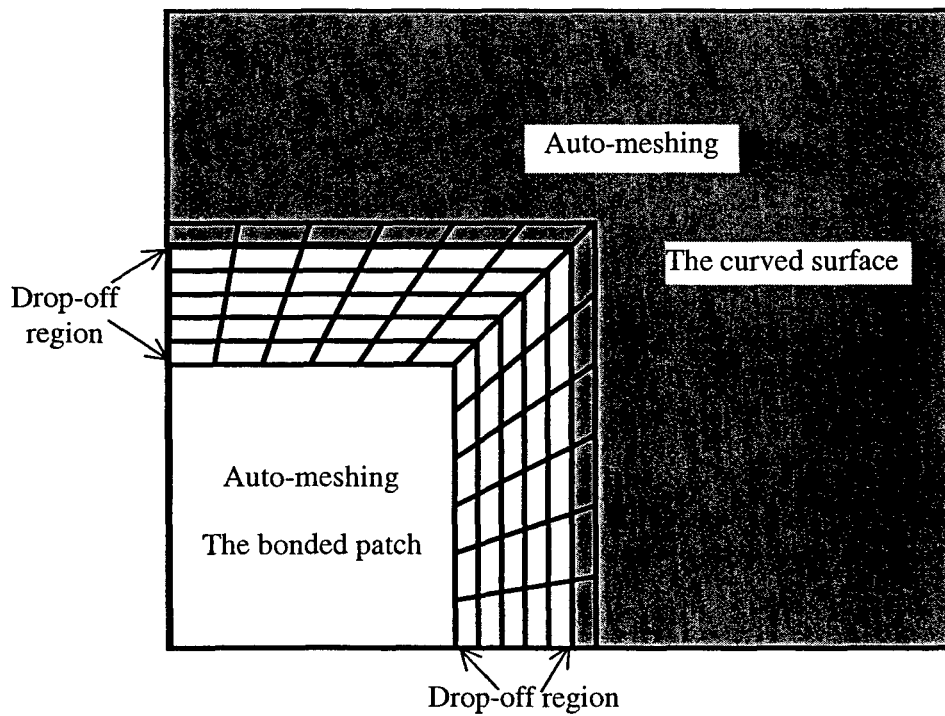
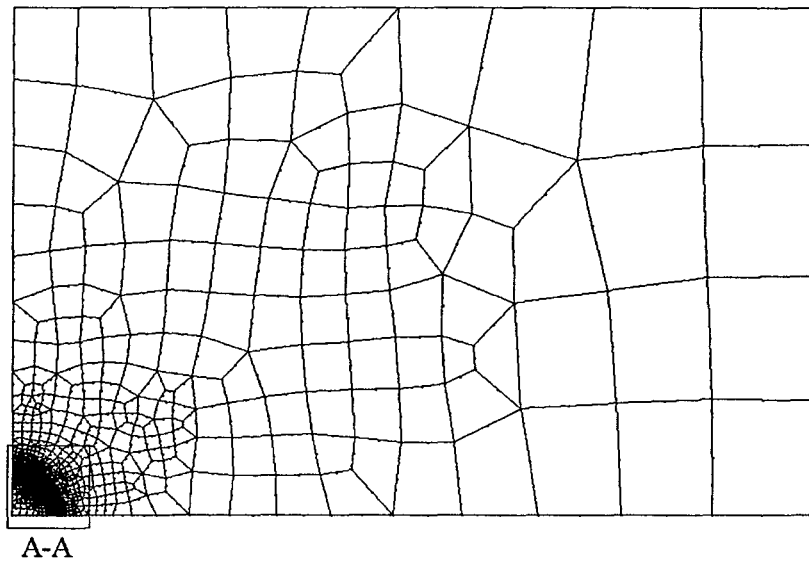
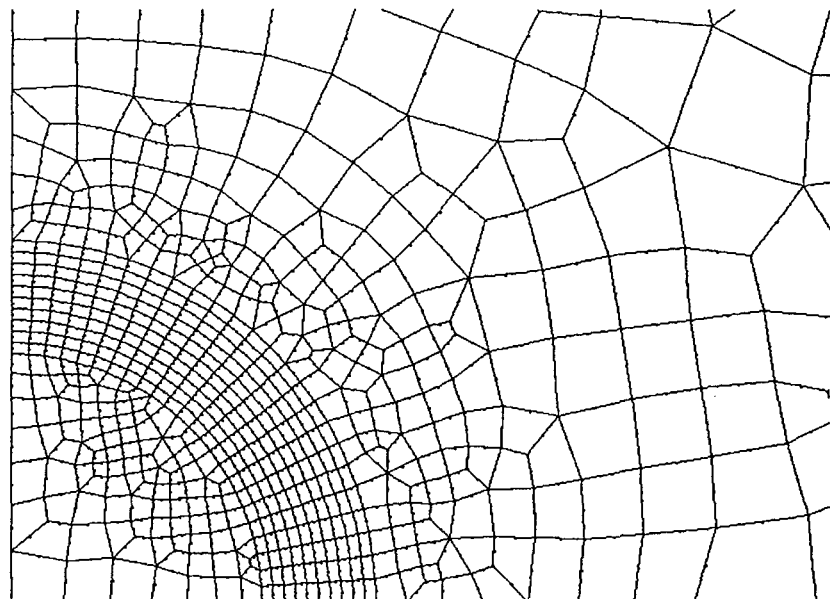


Figure 4-7 Mesh scheme for a square patch with the ply drop-offs (One quarter of structure)

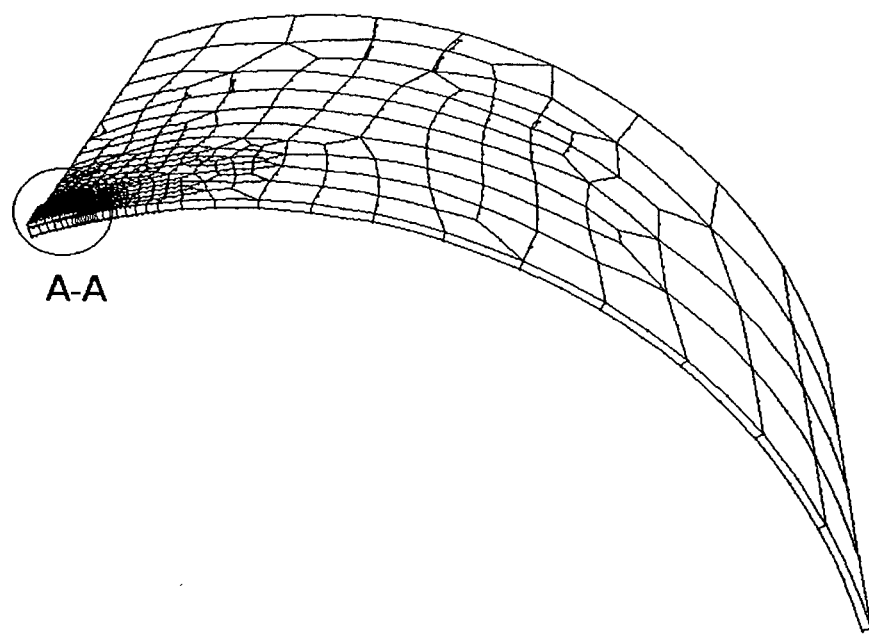


(a) Mesh in a flat plane

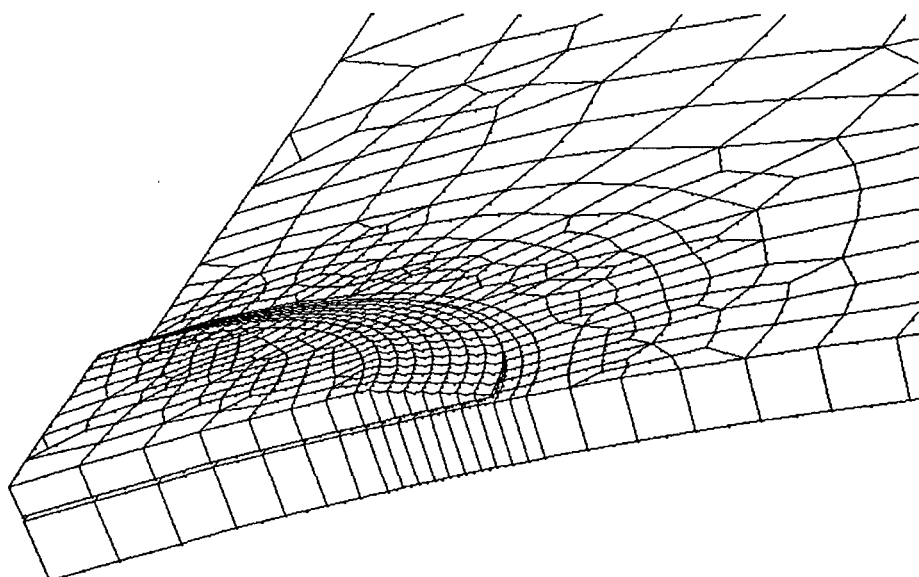


(b) local details of A-A

Figure 4-8 Mesh generated in a flat plane for a circle patch with ply drop-offs bonded to a cylindrical shell

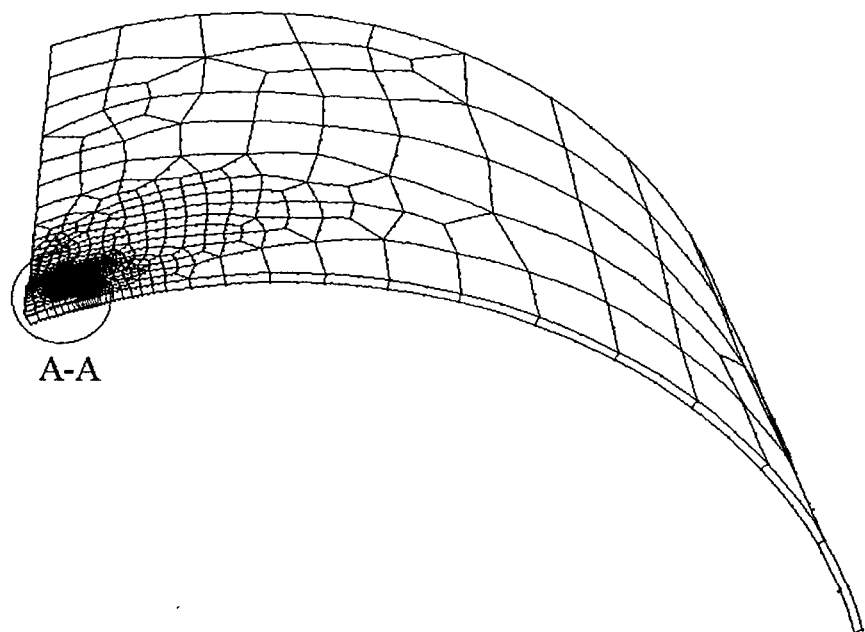


(a) Global view of structure

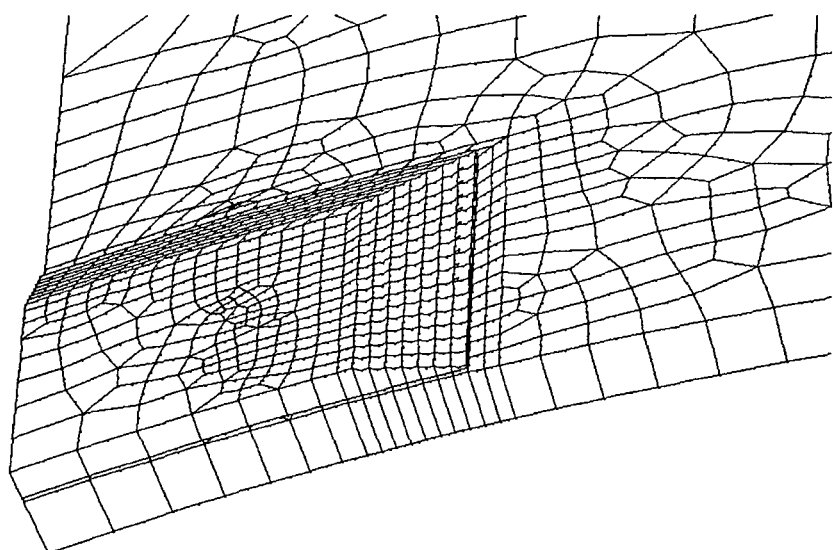


(b) Local details of A-A

Figure 4-9 Typical mesh for a circle patch with ply drop-offs bonded to a cylindrical shell

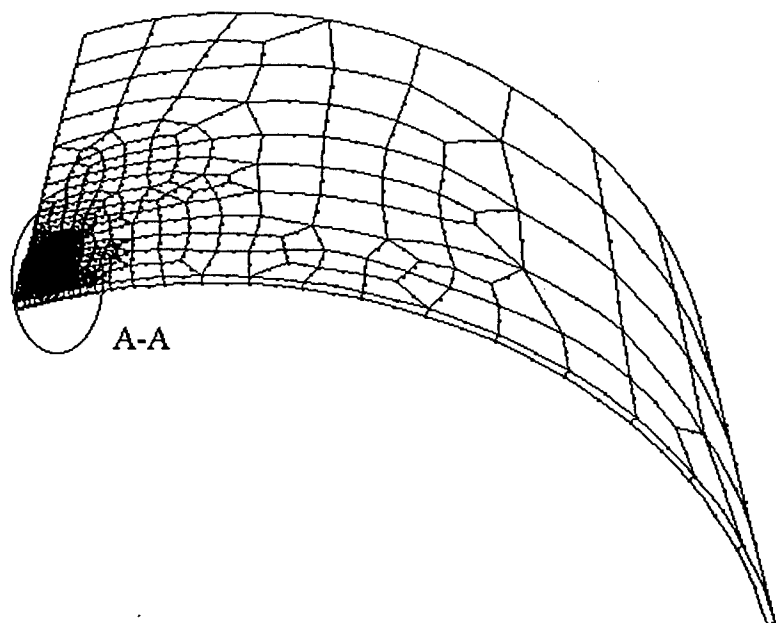


(a) Global view of structure

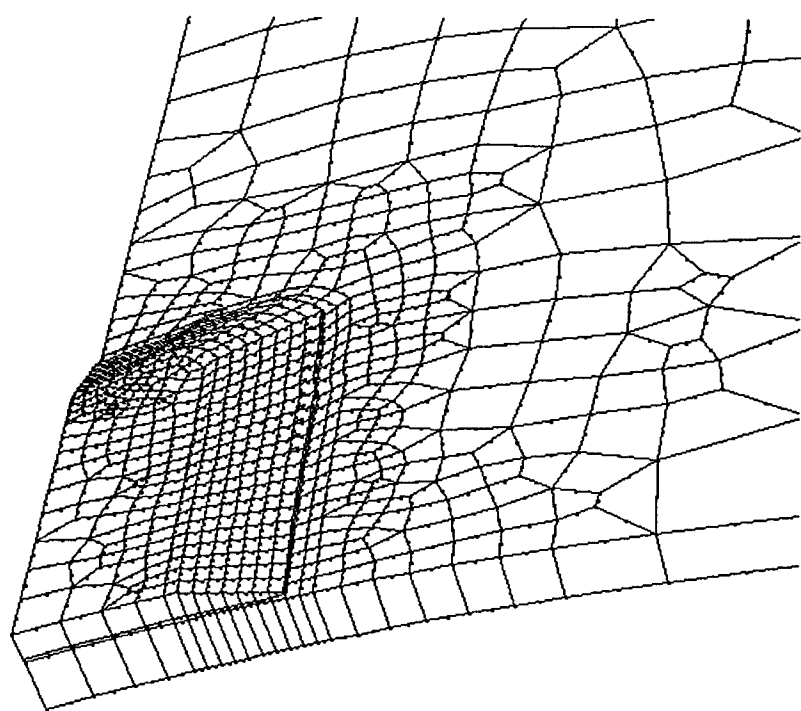


(b) Local details of A-A

Figure 4-10 Typical mesh for a square patch with ply drop-offs bonded to a cylindrical shell



(a) Global view of structure



(b) Local details of A-A

Figure 4-11 Typical mesh for the optimum shape of patch with ply drop-offs bonded to a cylindrical shell

4.4 Optimization method

Because only one single drop-off width is employed as the design variable, a one-dimensional direct search method is employed to find the optimum drop-off width. In this report, the 0.618 division method is used.

As shown in Figure 4-12, x is the optimization parameter and $f(x)$ is the objective function. It is possible that there may exist several peak values in the whole range of x and the maximum and minimum values of objective function can be obtained from these peak values. However, it is difficult to know how many peak values in the whole range of x . Therefore, the whole range of optimization parameter should be divided into several segments. For each segment, we can assume that there are only two peak values, which stand for the maximum and minimum value respectively. These two peak values can be searched iteratively by using the 0.618 division method. Then we can obtain the maximum or minimum value of objective function by comparing the peak values in these segments. Accordingly, the optimum ply drop-offs width is the corresponding width that minimizes the objective function.

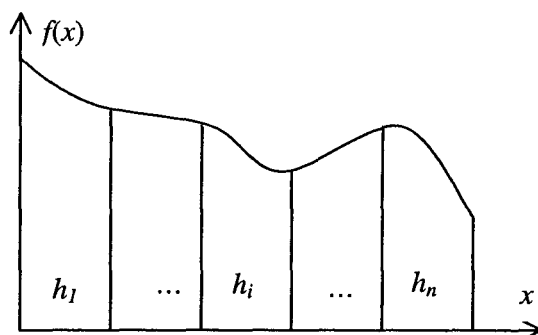


Figure 4-12 One-dimensional direct search scheme

4.5 Verification of the proposed FEA module

As shown in Figure 4-13, a cantilever curved beam bonded with a patch-beam is subjected to a tangent load T at its free end. The curvature radius of beam is $R=150\text{mm}$ and its sector angle is 30° . The circumferential length of the bonded patch-beam is 15.0mm . The thickness of the

parent beam and the patch-beam are 2.0mm and 1.0mm respectively. The thickness of adhesive layer is 0.15mm. The tangent load is equal to 1.0 N/mm.

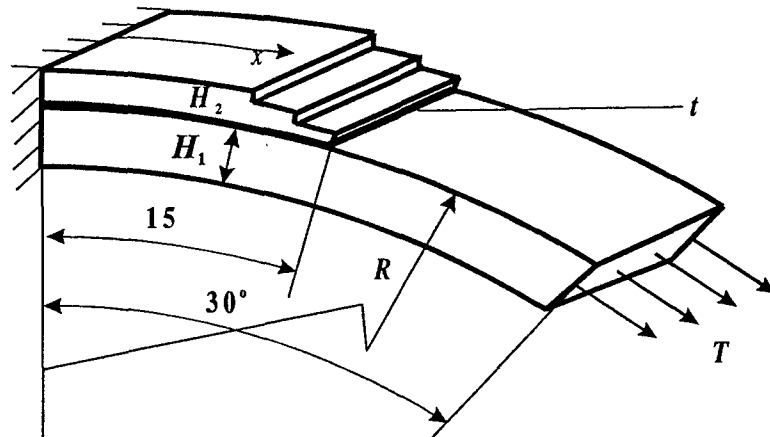


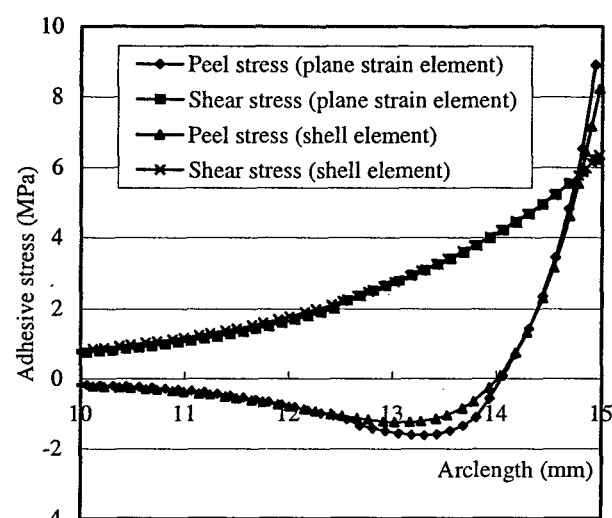
Figure 4-13 Cantilever curved beam with drop-offs subjected tangent load at its free end

Total 8 drop-offs are considered in the patch-beam. The uniform drop-offs width is 0.25mm. The circumferential length of drop-off region is 2.0mm. Both the parent beam and the patch-beam are assumed to be aluminum with a Young's modulus of $E=70\text{GPa}$ and a Poisson's ratio of $\nu=0.3$. The adhesive has a Young's modulus of $E_c=2.4\text{GPa}$ and a Poisson's ratio of $\nu_c=0.33$.

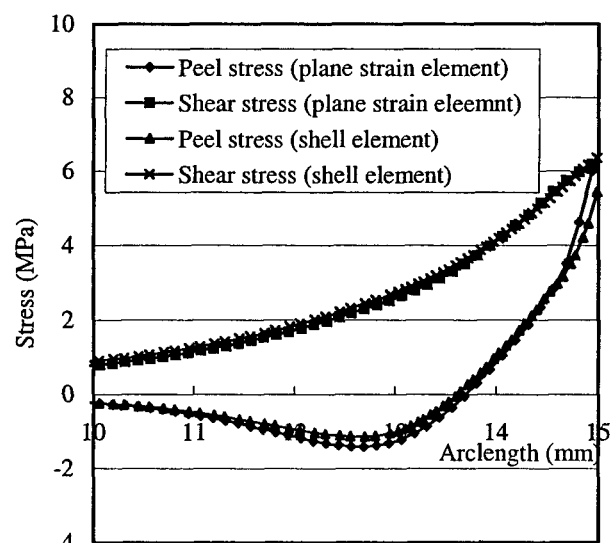
Commercial finite element analysis software STRAND 7 is used to analyze the problem and to serve as a benchmark for the proposed FEA module. Plane strain element is used to model both the beam (parent beam and patch-beam) and the adhesive layer. For the patch-beam, 8 elements are divided across the overall thickness and the same size 0.125mm is used in its circumferential direction. The same element size is applied to the parent beam. The circumferential size of the adhesive layer is 0.125mm too. Only one element is used across the adhesive layer's thickness. For the shell element in the proposed FEA module, the circumferential size is equal to the drop-off width. The width of beam is taken as 10mm for shell analysis.

Figure 4-14 depicts the adhesive stresses distribution near the free end of the overlap region along the circumferential direction for both with and without drop-off at the end of patch-beam. It can be seen that the predictions given by the present FEA module correlate well with the results of STRAND7.

An inspection of the peak values of the adhesive stresses in Figure 4-14 shows that the peak value of the peel stress decreases with the existence of drop-offs in the patch-beam, and the absolute value of compressive stress becomes smaller too. However, the peak value of the shear stress remains unchanged. The stress distribution patterns remain the same with the peak value near the end of the adhesive layer for both peel and shear stress.



(a) No ply drop-off



(b) Ply drop-off width=0.25mm

Figure 4-14 Adhesive tresses distribution along the circumferential direction

4.6. Numerical examples

The same cylindrical structure analyzed in 3.4 is considered to investigate the effect of the ply drop-offs of the bonded patch on the peak adhesive stresses. It should be noted that the patch is made of composite materials. The load and boundary condition are as the same as those given in Section 3.4.

The composite material used here is assumed to have the following properties

$$\begin{array}{lll} E_1 = 181.0 \text{GPa} & E_2 = E_3 = 10.3 \text{GPa} & G_{12} = G_{13} = 7.17 \text{GPa} \\ G_{23} = 4.02 \text{GPa} & \mu_{12} = \mu_{13} = 0.28 & \mu_{23} = 0.28 \end{array}$$

The stacking sequence of the composite patch are $[90_8]$, $[0_8]$, $[90/0/90/0]_s$ and $[0/90/0/90]_s$, respectively. The thickness of a single ply of composite is 0.127mm. Then the thickness of the patch is 1.016mm. Because only cross-plies are taken into account, we can take advantage of its structural symmetry to save the computational time by analyzing one quarter of the structure.

In the meantime, the uniform ply drop-offs width is defined for each ply drop-off step. To investigate the effect of the residual thickness (the thickness of the first drop-off step starting from the boundary of patch and adjacent to the adhesive layer), the residual thickness is defined as 1, 2 and 3 plies. Then total 7, 6 and 5 steps of ply drop-offs are considered accordingly.

Three shapes of the bonded patch are analyzed here, i.e., circular patch, rectangular patch and the optimum shape of patch obtained by the shape optimization analysis in Section 3. For circular and rectangular patches, $[90_8]$ and $[0_8]$ are analyzed. For the optimum shape of patch, $[90/0/90/0]_s$ and $[0/90/0/90]_s$ are considered.

It is obvious that the drop-off width cannot be enlarged unlimitedly because of the limited size of the bonded patch. The range of drop-off width is then given to avoid the unrealistic drop-offs. In this example, the uniform drop-off width for circular and square patch is from 0.1mm to 1.5mm. The total width of drop-off region can be in a range of 0.7mm to 10.5mm. For the

optimum shape of patch, the drop-off width is from 0.1mm to 1.0mm with a drop-off region ranging from 0.7mm to 7.0mm.

4.6.1 Circular patch

Figure 4-15 to Figure 4-20 depict the maximum normalized adhesive stresses for circular composite patch with different residual thickness with the ply lay-up $[0_8]$, $[90_8]$. The maximum adhesive stresses with and without ply drop-off are defined as σ_{\max} and $\sigma_{\max 0}$, respectively.

From Figure 4-15 to 4-17, it is obvious that the introduction of ply drop-off can reduce the stress concentration quite remarkably. The maximum peel stress for $[0_8]$ patch with the residual thickness 0.127mm is only 21.2% of its initial value when the ply drop-off width is 1.5mm (see Figure 4-13). 62.2% and 60.1% of the initial values exist for the maximum shear and Von Mises stresses under the same condition. The maximum stresses are decreased by 78.8%, 37.8% and 39.9%, respectively. It is easy to find that the maximum peel stress is reduced much more than the maximum shear and Von Mises stress for the same drop-off width. In fact, the applied load is mainly transferred from the cylindrical shell to the bonded patch by shear stresses in the adhesive layer, and thus the shear stress cannot be reduced dramatically.

However, the maximum stresses don't continuously decrease with the extension of the ply drop-off width. At certain stage, the maximum stresses may increase slightly with an increasing drop-off width. For the $[90_8]$ patch shown in Figure 4-18 to 4-20, the maximum peel stress decreases at first (drop-offs width=0.0 – 0.15mm), then it increase with the drop-off width in the range of 0.15mm to 0.6mm, and eventually the peel stress decrease again. This shows that it is necessary to choose proper drop-off width by optimization analysis to minimize the peak value of adhesive stresses.

Comparing the stress level for different residual thickness of the patch, it can be easily found that the objective stresses for the thicker residual thickness are generally higher than that for thinner residual thickness with the same drop-offs width. This shows that the thinner residual thickness results in more reduction in adhesive stress.

On the other hand, the effect of ply drop-off on the adhesive stresses changes with the stacking sequence of composite patch. For the same drop-off width and same residual thickness, the adhesive stresses of $[0_8]$ patch are reduced much more than that of $[90_8]$ patch. As clearly shown in Table 4-1, the adhesive stresses of $[0_8]$ patch are much lower than that of $[90_8]$ patch. It indicates that the effect of ply drop-off for the $[0_8]$ patch is more remarkable than that for the $[90_8]$ patch for this load case.

It can also be seen that there are some uncontinuous points in these curves in Figure 4-15 to 4-20. This is because the position of the maximum adhesive stresses in the bonded patch changes with different ply drop-off width. Table 4-2 shows the coordinate of the maximum adhesive stresses $[0_8]$ patch with different ply drop-off width.

4.6.2 Square patch

The results of maximum adhesive stresses for square patch are given from Figure 4-21 to 4-26. It can be seen that the maximum peel and Von Mises stress are reduced in similar fashion as that of circular patch. For the $[0_8]$ patch, the adhesive stresses of square patch are reduced slightly less than that of the circular patch with the same drop-offs width and residual thickness. However, for the $[90_8]$ patch, the adhesive stresses of the square patch are reduced slightly more than that of the circular patch with the same drop-off width and residual thickness. This shows that the effect of ply drop-off is affected by the stacking sequence of composite patch.

It should be noted that the maximum shear stress of the $[0_8]$ square patch increases with the introduction of small ply drop-off (see Figure 4-21 to 4-23). For the residual thickness equal to 0.381mm, the maximum shear stress remains larger than that without drop-off. This is because we define the maximum shear stress as a combination of two components τ_{yz} , τ_{xz} , which is given in equation (3-13). The ply drop-off decreases the component τ_{yz} for the whole range of drop-off width. But the component τ_{xz} increases rapidly with a very short drop-off width, which is caused by the load and boundary condition. Meanwhile, the position of the maximum shear stress is different too. The numerical results show that thinner residual thickness is preferred.

4.6.3 Patch with the optimum shape

To investigate the effect of ply drop-offs on the patch with the optimum shape obtained by shape optimization in Section 3, two types of stacking sequences of composite patches, $[90/0/90/0]_s$ and $[0/90/0/90]_s$, are analyzed using the presented module. The maximum adhesive stresses with different ply drop-off width for these two patches are shown in Figure 4-27 and 4-28.

Obviously, the existence of ply drop-off can reduce the maximum adhesive stresses for these two cross-ply patches. But it can be seen that the maximum peel stress for $[0/90/0/90]_s$ decreases first, then increases dramatically and finally decreases. It is evident that it should be careful to introduce drop-off to composite patch bonded to a curved surface. The adhesive stresses may increase if the drop-off width is not adequately selected, which clearly demonstrate the necessity of optimal selection of tapering.

Table 4-1 Maximum adhesive stresses with the optimum drop-off of composite patch (residual thickness=0.127mm)

Patch shape	Lay-up of patch	Drop-off width	Maximum peel stress	Maximum shear stress	Maximum Von Mises stress
Circle	$[0_8]$	0.0	11.37 (0.98, 14.96)	9.43 (9.13, 11.90)	10.18 (1.96, 14.87)
		1.5	2.42 (0.00, 15.00)	5.87 (15.00, 0.00)	6.11 (15.00, 0.00)
	$[90_8]$	0.0	14.79 (0.0, 15.00)	20.06 (0.50, 14.99)	21.80 (0.00, 15.00)
		1.5	8.23 (0.00, 15.00)	17.17 (0.00, 15.00)	17.82 (0.00, 15.00)
Square	$[0_8]$	0.0	9.47 (2.00, 15.00)	7.33 (13.50, 15.00)	9.09 (13.50, 15.00)
		1.5	2.55 (14.00, 15.00)	5.90 (15.00, 15.00)	5.91 (15.00, 15.00)
	$[90_8]$	0.0	17.10 (14.50, 15.00)	20.61 (14.00, 15.00)	22.71 (14.00, 15.00)
		1.5	7.34 (9.00, 15.00)	15.71 (9.00, 15.00)	16.28 (9.00, 15.00)
Optimum shape	$[90/0/90/0]_s$	0.0	9.52 (16.97, 8.77)	15.42 (19.95, 8.48)	16.01 (16.97, 8.77)
		1.0	4.72 (12.98, 9.02)	12.94 (13.98, 9.00)	13.21 (13.98, 9.00)
	$[0/90/0/90]_s$	0.0	12.58 (13.98, 9.00)	14.61 (19.95, 8.48)	15.94 (16.97, 8.77)
		1.0	10.49 (13.98, 9.00)	10.18 (13.98, 9.00)	11.85 (13.98, 9.00)

Table 4-2 Position of maximum adhesive stresses in the [0₈] circle patch with residual thickness=0.127mm

Drop-offs width (mm)	Maximum peel stress (MPa)	x (mm)	y (mm)	Maximum shear stress (MPa)	x (mm)	y (mm)	Maximum Von Mises stress (MPa)	x (mm)	y (mm)
0.00	11.37	0.98	14.96	9.43	9.13	11.90	10.18	1.96	14.87
0.10	8.57	0.00	15.00	7.63	9.13	11.90	8.27	4.82	14.20
0.15	8.30	0.00	15.00	7.51	9.13	11.90	8.07	4.82	14.20
0.20	7.75	0.00	15.00	7.38	9.13	11.90	7.82	4.82	14.20
0.25	7.15	0.00	15.00	7.22	9.13	11.90	7.54	4.82	14.20
0.30	6.57	0.00	15.00	7.05	9.13	11.90	7.25	5.74	13.86
0.35	6.07	0.00	15.00	6.88	9.89	11.28	6.99	5.74	13.86
0.40	5.65	0.00	15.00	6.75	9.89	11.28	6.94	15.00	0.00
0.45	5.27	0.00	15.00	6.63	10.61	10.61	6.91	15.00	0.00
0.50	4.91	0.00	15.00	6.51	11.28	9.89	6.88	15.00	0.00
0.55	4.64	0.00	15.00	6.42	11.90	9.13	6.84	15.00	0.00
0.60	4.39	0.00	15.00	6.35	12.47	8.33	6.80	15.00	0.00
0.65	4.16	0.00	15.00	6.32	15.00	0.00	6.78	15.00	0.00
0.70	3.96	0.00	15.00	6.29	15.00	0.00	6.73	15.00	0.00
0.75	3.79	0.00	15.00	6.29	15.00	0.00	6.72	15.00	0.00
0.80	3.63	0.00	15.00	6.26	15.00	0.00	6.68	15.00	0.00
0.85	3.50	0.00	15.00	6.24	15.00	0.00	6.64	15.00	0.00
0.90	3.38	0.00	15.00	6.22	15.00	0.00	6.61	15.00	0.00
0.95	3.27	0.00	15.00	6.19	15.00	0.00	6.57	15.00	0.00
1.00	3.16	0.00	15.00	6.16	15.00	0.00	6.53	15.00	0.00
1.05	3.07	0.00	15.00	6.12	15.00	0.00	6.47	15.00	0.00
1.10	2.98	0.00	15.00	6.09	15.00	0.00	6.43	15.00	0.00
1.15	2.89	0.00	15.00	6.07	15.00	0.00	6.39	15.00	0.00
1.20	2.82	0.00	15.00	6.05	15.00	0.00	6.35	15.00	0.00
1.25	2.75	0.00	15.00	6.04	15.00	0.00	6.33	15.00	0.00
1.30	2.68	0.00	15.00	6.01	15.00	0.00	6.29	15.00	0.00
1.35	2.60	0.00	15.00	5.98	15.00	0.00	6.26	15.00	0.00
1.40	2.53	0.00	15.00	5.93	15.00	0.00	6.19	15.00	0.00
1.45	2.48	0.00	15.00	5.91	15.00	0.00	6.16	15.00	0.00
1.50	2.42	0.00	15.00	5.87	15.00	0.00	6.11	15.00	0.00

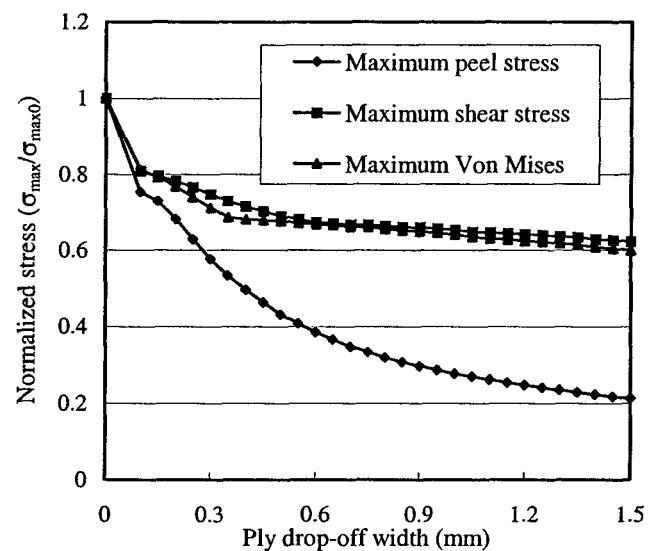


Figure 4-15 The maximum stresses for $[0_8]$ circular composite patch with the residual thickness=0.127mm

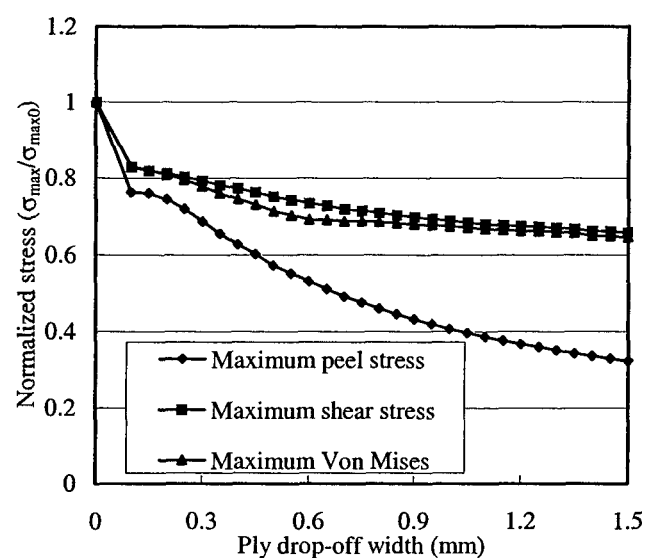


Figure 4-16 The maximum stresses for $[0_8]$ circular composite patch with the residual thickness=0.254mm

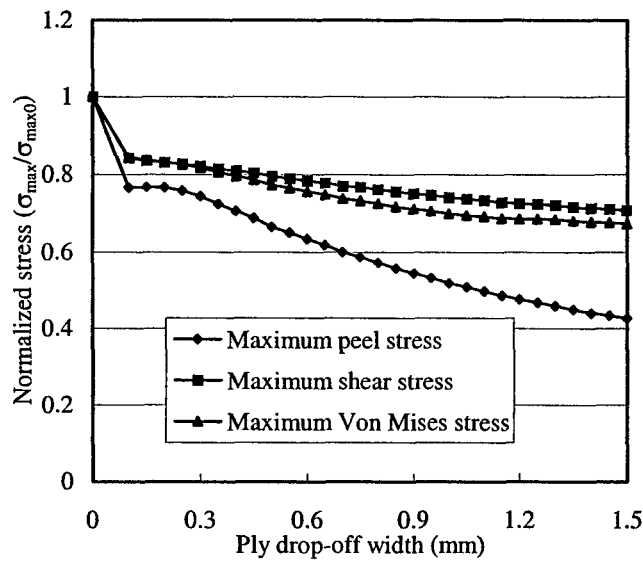


Figure 4-17 The maximum stresses for $[0]_8$ circular composite patch with the residual thickness=0.381mm

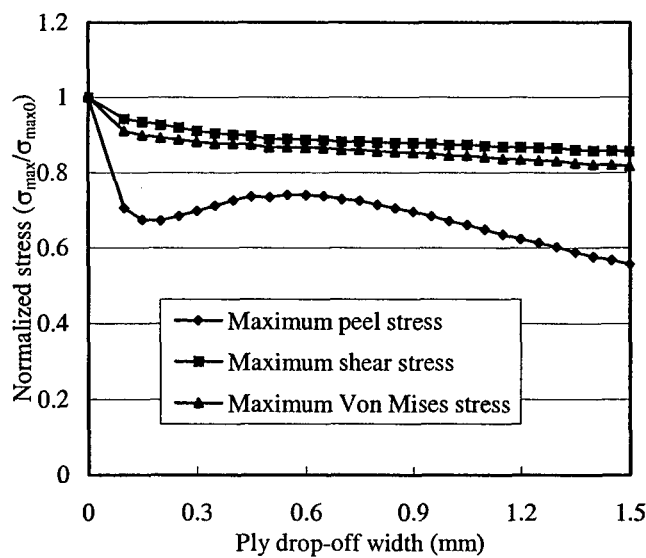


Figure 4-18 The maximum stresses for $[90]_8$ circular composite patch with the residual thickness=0.127mm

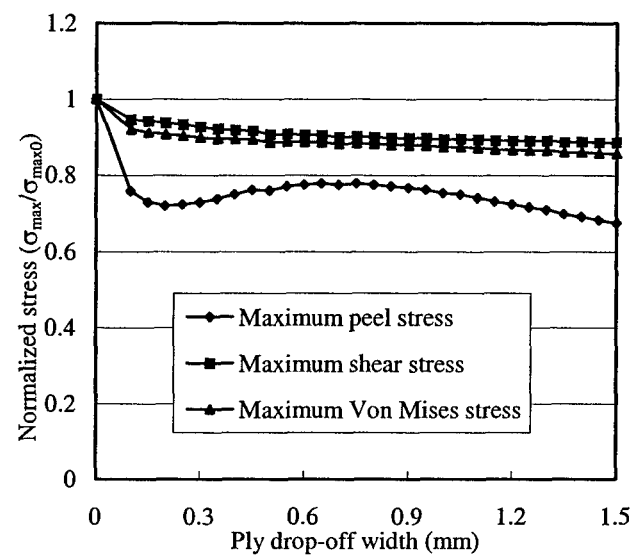


Figure 4-19 The maximum stresses for [90]₈ circular composite patch with the residual thickness=0.254mm

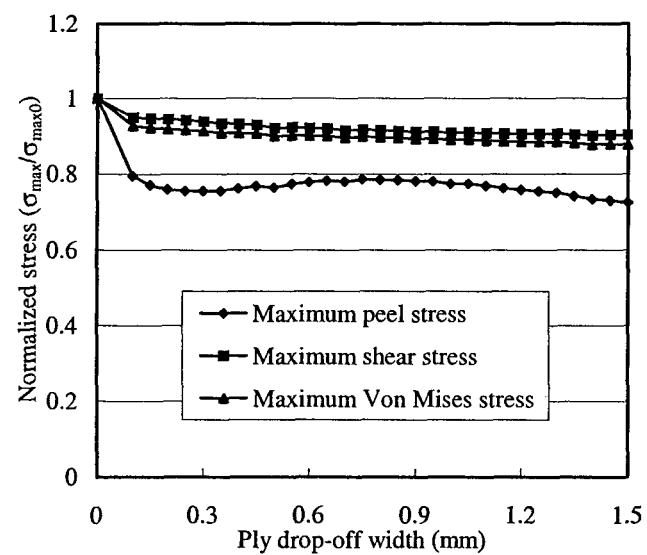


Figure 4-20 The maximum stresses for [90]₈ circular composite patch with the residual thickness=0.381mm

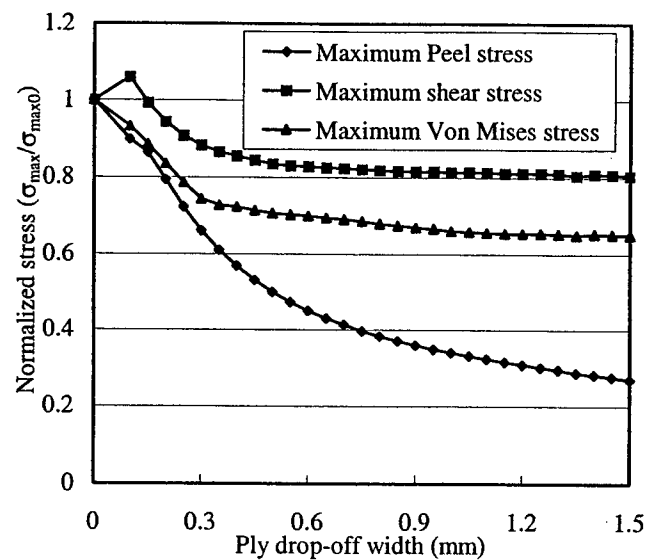


Figure 4-21 The maximum stresses for $[0_8]$ square composite patch with the residual thickness=0.127mm

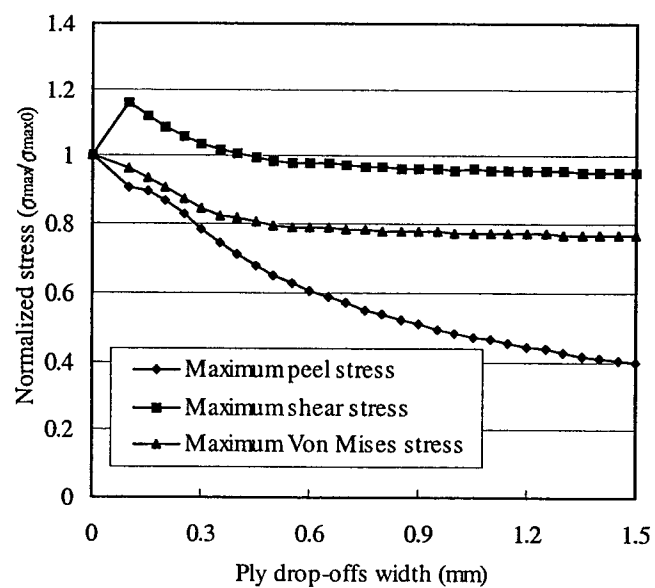


Figure 4-22 The maximum stresses for $[0_8]$ square composite patch with the residual thickness=0.254mm

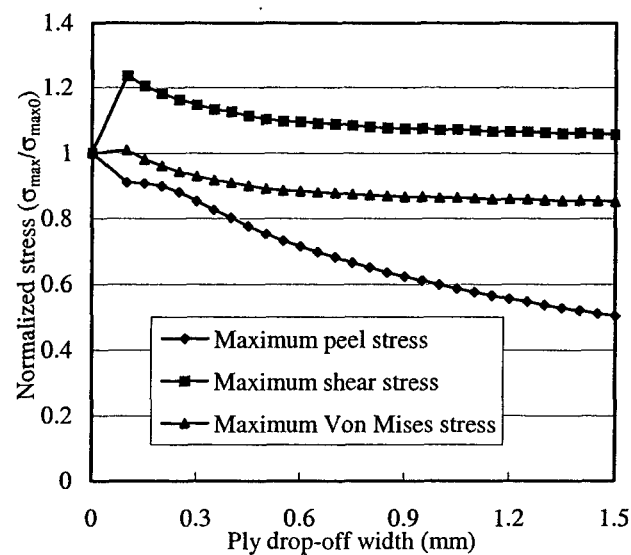


Figure 4-23 The maximum stresses for $[0_8]$ square composite patch with the residual thickness=0.381mm

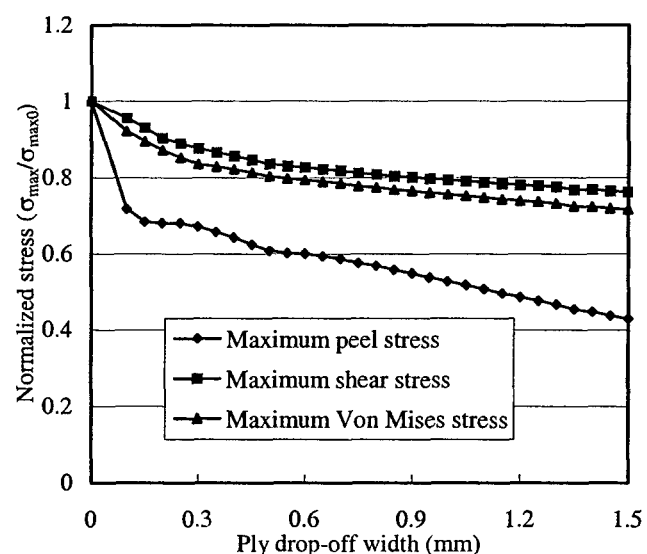


Figure 4-24 The maximum stresses for $[90_8]$ square composite patch with the residual thickness=0.127mm

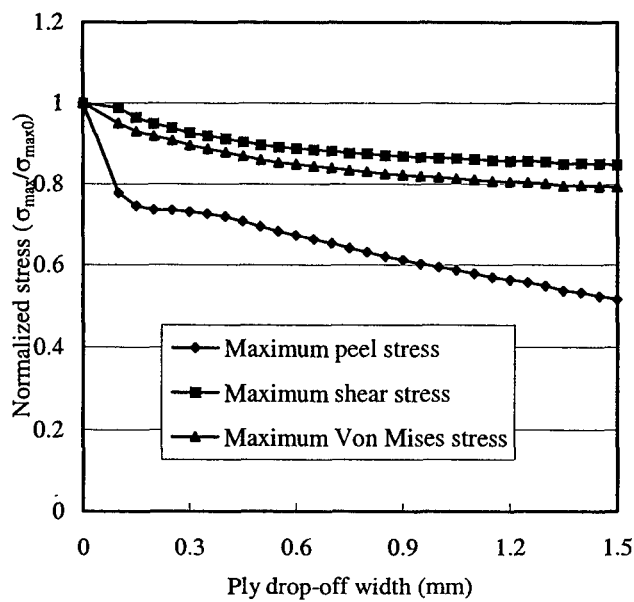


Figure 4-25 The maximum stresses for $[90_8]$ square composite patch with the residual thickness=0.254mm

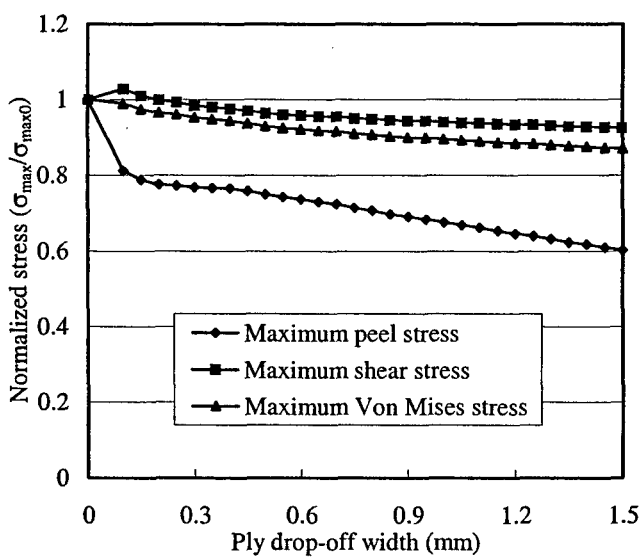


Figure 4-26 The maximum stresses for $[90_8]$ square composite patch with the residual thickness=0.381mm

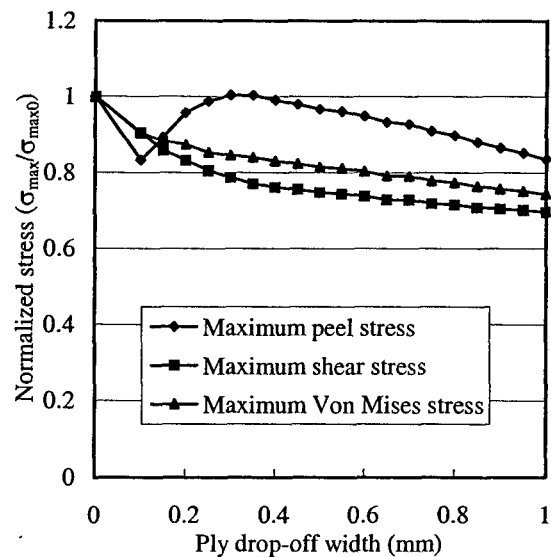


Figure 4-27 The maximum stresses for optimum shape of $[0/90/0/90]_s$ composite patch

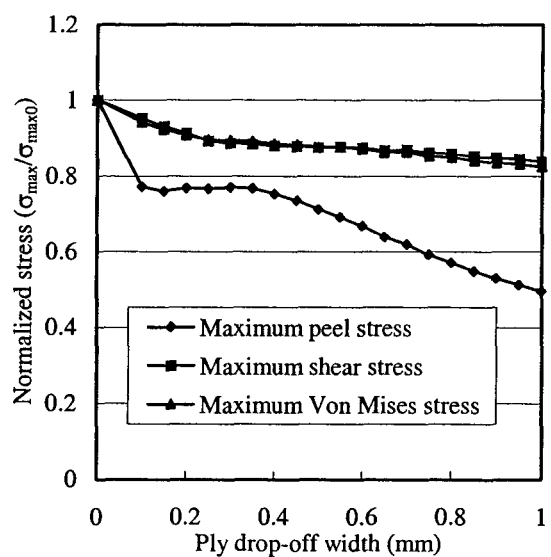


Figure 4-28 The maximum stresses for optimum shape of $[90/0/90/0]_s$ composite patch

5. Optimization of the ply lay-ups of a composite bonded patch

As mentioned in Section 4, the alternative approach to improve the stress concentration on the interface between the different materials is to choose an appropriate combination of material constants for the two candidate materials when the geometry is fixed. Although this combination can be theoretically found, it is not easy to implement because of the limitation of available materials. Therefore, this concept is not widely applied to the metal patch. However, composite materials enable us to adjust the global properties of a laminate remarkably by changing its ply lay-ups. So it is practically desirable to search for optimum ply lay-ups to reduce the stress concentration in the adhesive layer.

In the current analysis, the SLP method is employed to conduct the optimization analysis of the ply lay-ups of a composite bonded patch. The objective is to minimize the adhesive stresses and the design variables are the fiber orientation angles of all plies in the composite patch. The shape and thickness of the bonded patch are assumed fixed. The analysis approach is presented first and follows some numerical examples.

5.1. Optimization method

The SLP method, briefly described in 3.1, is applied to conduct the optimization analysis. The formulations used are given in the following.

5.1.1 Objective function

The purpose of optimization is to minimize the adhesive stresses. So the adhesive stresses are selected as the objective function. Here, the maximum peel stress and Von Mises stress (see equation (3-9) and (3-11)) in the adhesive layer are used as the objective function, respectively.

5.1.2 Design variables

Only the fiber orientation angles of every ply in the composite patch are chosen to be design variables and they are assumed to take values of full degree(s) between -90 and 90 degree(s).

The shape and thickness of the bonded patch are not design variables and they are assumed to be fixed in the current analysis.

5.1.3 Sensitivity analysis

The sensitivity analysis for the ply lay-ups optimization is basically similar to that for the shape optimization in equation (3-6). The difference is how to calculate the increment of the global stiffness and applied load.

Because only the fiber orientation angles of all plies in the composite patch are the design variables, we only need to calculate the increment of the global stiffness and load caused by the change of fiber orientation.

As assumed above, the shape and thickness of the bonded patch are fixed in the whole analysis, i.e., the geometry of structure keeps unchanged. This results in that there is no change of the applied load. Therefore, we have

$$\Delta P = P' - P = 0 \quad (5-1)$$

For the change of fiber orientation of each ply in the composite patch, the elastic matrix of bonded patch is changed accordingly

$$D' = D + \Delta D \quad (5-2)$$

where D' is the elastic matrix of bonded patch with new ply-ups. D is the elastic matrix of composite patch before the ply orientation angle is changed. ΔD is the increment elastic matrix.

For the differentiation of stiffness, we have

$$\begin{aligned} \Delta K &= \int_{\Omega} B^T D' B d\Omega - \int_{\Omega} B^T D B d\Omega \\ &= \int_{\Omega} B^T (D + \Delta D) B d\Omega - \int_{\Omega} B^T D B d\Omega \end{aligned} \quad (5-3)$$

where Δk is the increment global stiffness matrix caused by the change of fiber orientation angle. The rest terms are the same as are given in equation (3-7).

Then the displacements, before and after the fiber orientation is changed, can be obtained as follows

$$\begin{aligned} q &= K^{-1}P \\ q' &= (K')^{-1}P' = (K + \Delta K)^{-1}P \end{aligned} \quad (5-4)$$

Ignoring the second small term and following the similar procedure from equation (3-4) to (3-6), the variation of displacements caused by the change of the fiber orientation angle can be given by

$$\Delta q = q' - q = -K^{-1}\Delta K q \quad (5-5)$$

Then substituting equation (5-5) into equation (3-8), we can obtain all the stress sensitivities at a node or a Gaussian point for every change of fiber orientation. It is worth pointing out that x_i stands for the fiber orientation angle of the i th ply in the composite bonded patch here.

5.1.4 Constraints

It is obvious that the stress constraints for the optimization of the ply lay-ups are the same as those for the shape optimization described in Section 3. Therefore, we have

$$\sigma_i^{(k-1)} + \sum_{j=1}^n \frac{\partial \sigma_i^{(k)}}{\partial x_j} (x_j^{(k)} - x_j^{(k-1)}) < \sigma_{\max}^{(k-1)} \quad (i = 1, \dots, m, \quad j = 1, \dots, n) \quad (5-7)$$

where n is the number of plies in the bonded patch and x denotes the fiber orientation angle. The rest terms are as same as those in equation (3-15).

Similarly, the objective function is given by

$$\sum_{j=1}^n \frac{\partial \sigma_{j \max}^{(k)}}{\partial x_j} (x_j^{(k)} - x_j^{(k-1)}) \quad (5-8)$$

For each ply of the composite bonded patch, the fiber orientation angle is limited in a range of -90 to +90 degrees because of the periodical characteristics of composite material. Then we have

$$-90 < x_j^{(k)} < 90 \quad (j = 1, \dots, n) \quad (5-9)$$

Finally, a move limit is imposed to design variables

$$-d < x_j^{(k)} - x_j^{(k-1)} < d \quad (5-10)$$

It is worth noting that the optimization scheme presented above may result in an arbitrary stacking sequence of composite patch. Then the symmetry across the thickness of optimal patch cannot be maintained. However, symmetrical lay-ups of composite patch are generally applied in engineering structure. One more constraint, therefore, is imposed for simplicity to the optimization method. The corresponding two symmetrical plies (refer to the mid-plane of the composite patch) are assumed to change in a same angle in each iteration step.

5.2 Numerical example

The cylindrical structure described in Section 3.4 is taken to study optimization of the ply lay-ups of composite patch. Both ends of the cylindrical shells are fixed to three translation displacements, which allow rotational displacements only. An internal pressure $p=1.0\text{MPa}$ is applied to the cylindrical shell.

The same material is applied to the cylindrical shell and the adhesive layer with thickness 2.0mm and 0.15mm respectively. Other size of cylindrical shell is as same as that given in 3.4. The composite patch has the same material properties as given in Section 4.6.

Two kinds of shape of patch are considered here, which are circle and square patches. The initial stacking sequences of the bonded patch are $[90_{16}]$ and $[90_8]$. The thickness of a single ply is assumed to be 0.127mm. The total thickness of the patch is 2.032mm and 1.016mm, respectively.

The move limit is set to be 5.0 degree in each new iteration step. The move limit will be reduced to half of former value if the new objective stresses after changing the fiber orientation are higher than that in the last step. The calculation will be terminated if the difference of objective stresses between the current step and last step is smaller than 10^{-4} or the move limit is smaller than 10^{-1} .

Numerical results show that the optimum values of the adhesive stresses and optimal lay-ups are dependent of the initial values of fiber orientations. This clearly indicates the complex dependency of the objective adhesive stress on the ply lay-ups. To obtain a global optimal solution to the problem, evolutionary types of methods, such as Genetic Algorithm (GA), may be necessary. However, it is extremely computational expensive for the present problem because structural symmetry can no longer be used in each finite element analysis.

To illustrate the algorithm, a very simple example is considered, in which all the fiber are aligned in one direction, i.e., uni-directional composite patch. In this case, there is only one design variable, i.e., the angle between the fiber direction and the longitudinal direction of the shell.

Figure 5-1 to Figure 5-4 depicts the maximum adhesive stresses with different stacking angle and thickness of uni-direction patch of circular or square shape. From these figures, it is seen that the fiber direction affects the maximum adhesive stress in a very complicate manner, especially for the square patch. It is noted that the maximum peel stress has several stationary values ranging as the fiber angle from 0° to 90° for both shapes of patch. The maximum Von Mises stress has several stationary values too for the square patch. Table 5-1 gives the optimum maximum adhesive stress and optimum lay-ups of composite patch with the maximum peel stress and Von Mises stress being the objective function, respectively. Although 0° fiber can lead to a minimum peak value of Von Mises stress, the peel stress is

very high. Once again, it is necessary to determine the proper lay-ups according to the failure mode of adhesive layer. For example, if peel stress causes failure, the optimum fiber orientation is 50° for the circular patch, 60° for the square patch of 2.032mm thick and 0° for the square patch 1.016mm thick.

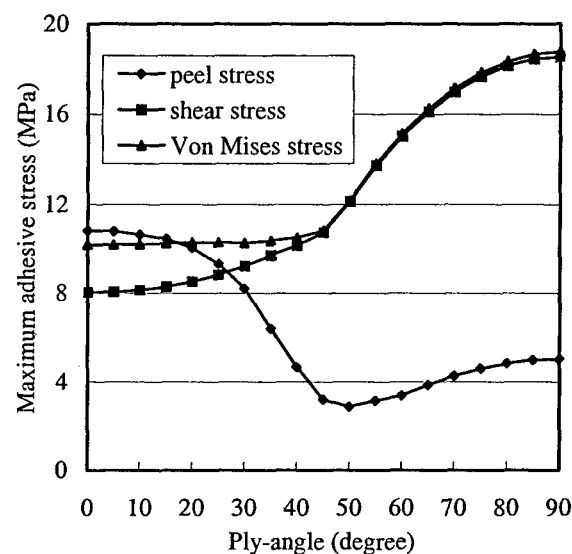


Figure 5-1 The maximum adhesive stresses with different stacking angle of uni-direction circle patch (thickness=2.032mm)

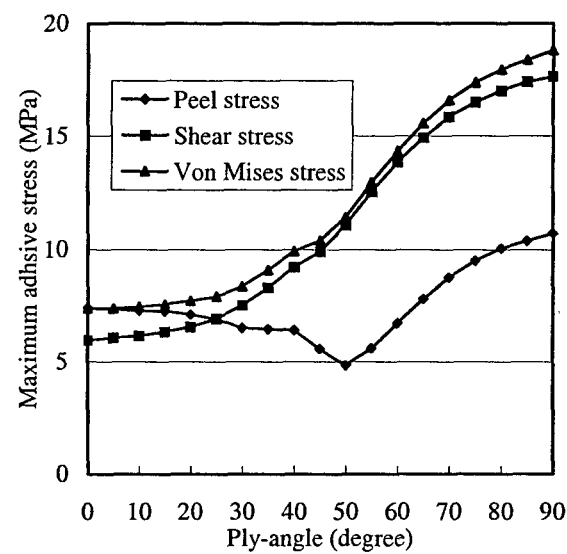


Figure 5-2 The maximum adhesive stresses with different stacking angle of uni-direction circle patch (thickness=1.016mm)

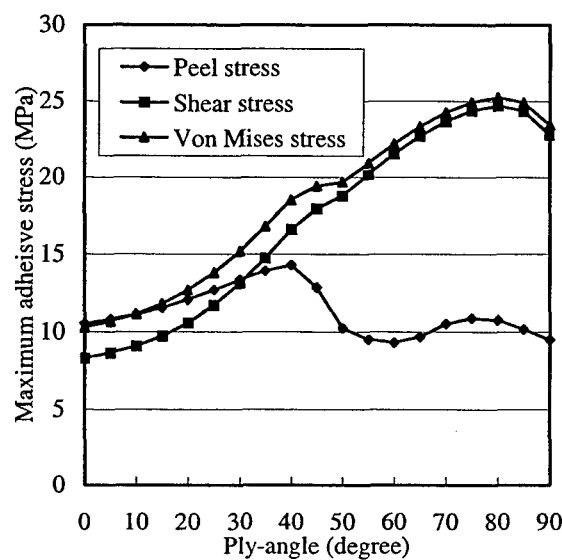


Figure 5-3 The maximum adhesive stresses with different stacking angle of uni-direction square patch (thickness=2.032mm)

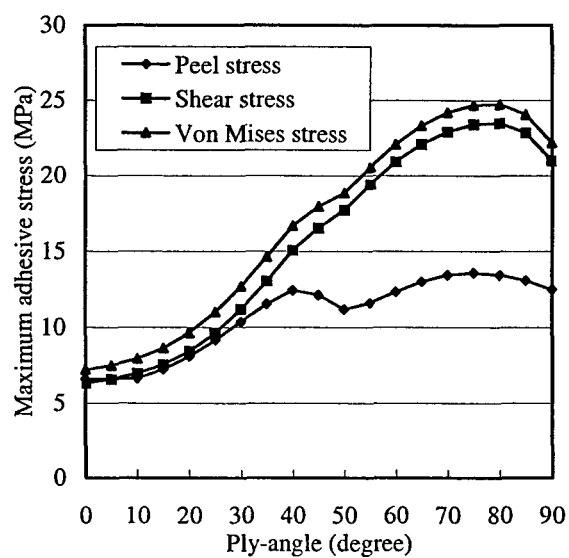


Figure 5-4 The maximum adhesive stresses with different stacking angle of uni-direction square patch (thickness=1.016mm)

Table 5-1 The optimum maximum adhesive stress and optimum lay-ups of uni-direction composite patch with different objective function

Shape of patch	Objective function	Lay-ups	Peel stress (MPa)	Shear stress (MPa)	Von Mises stress (MPa)
Circle	Initial*	[90 ₁₆]	5.04	18.53	18.76
	Peel stress	[50 ₁₆]	2.87	12.13	12.17
	Von Mises stress	[0 ₁₆]	10.83	8.05	10.20
Circle	Initial	[90 ₈]	10.73	17.64	18.80
	Peel stress	[50 ₈]	4.83	11.08	11.43
	Von Mises stress	[0 ₈]	7.38	5.96	7.37
Square	Initial	[90 ₁₆]	9.49	22.79	23.44
	Peel stress	[60 ₁₆]	9.32	21.53	22.19
	Von Mises stress	[0 ₁₆]	10.54	8.31	10.30
Square	Initial	[90 ₈]	12.48	21.00	22.20
	Peel stress	[0 ₈]	6.57	6.32	7.20
	Von Mises stress	[0 ₈]	6.57	6.32	7.20

*Initial lay-ups of optimization

6. CONCLUSIONS

In this report, a parametric optimization analysis has been conducted for optimal design of composite bonded patch repair to curved surface. Sequential Linear Programming (SLP) method and one-dimensional direct search method are employed as the optimization algorithm in conjunction with a fully implemented mesh generation algorithm into which new features were incorporated. Three types of design parameter are considered independently, which are: (a) geometrical shape of bonded patch, (b) ply drop-offs contour of bonded composite patch, (c) fiber orientation of each ply in bonded composite patch. The present study demonstrates the following salient points:

- (1) The geometrical shape of bonded patch to a curved surface affects the maximum adhesive stresses significantly. It is useful and practical to select an optimal shape of bonded patch to minimize the maximum adhesive stresses, which makes the adhesive layer more reliable and sustain higher loading.
- (2) It is assumed that there are only three out-of-plane stress components in the adhesive layer, i.e., peel stress and two shear stresses. These two shear stresses can be transformed into a single one shear stress. According the optimization analysis, the peel stress can be reduced much more than shear stress does, which can be seen for all three kinds of optimization analysis. This is because the applied load is mainly transferred by shear stress in the adhesive layer from the parent structure to the bonded patch.
- (3) Three kinds of objective function are considered, which are the maximum peel stress, the maximum shear stress and the maximum Von Mises stress. It can be seen that the optimal patches may be similar or vary when different objective functions are used. But it should be pointed that it is necessary to choose a proper objective function according to its actual failure mode to determine the final optimal patch.
- (4) An automatic mesh generation algorithm is fully implemented with some new features being incorporated into. The present mesh scheme can fully fulfill the requirement of stress analysis and optimization evolution for bonded patch design.
- (5) Nodal stress and Gaussian Stress may lead to similar and slightly different optimum patch when used as objective function being used. Due to the nature of stress concentration along the boundary of the patch, it is believed that accurate nodal stress should be used as objective function.
- (6) The introduction of ply drop-off in a bonded composite patch can dramatically reduce the peel stress. However, the Von Mises stress may also increase because of ply drop-

offs. Therefore, one should be careful to apply this method to reduce the adhesive stress.

- (7) The effect of the residual thickness of patch with ply drop-offs may vary with the stacking sequence and the shape of composite patch.
- (8) The effect of fiber orientation on the maximum adhesive stresses is very complicate. According to the analysis, there exist several peak values in the whole design range of fiber direction, even for a uni-direction composite patch. The current method, SLP, can only present a local optimal solution efficiently. However, because of the required computational time, it is unacceptable to search for a global optimal solution by available global optimization method. Consequently, only a local optimal solution is given in this report.

ACKNOWLEDGEMENT

The authors wish to acknowledge valuable technical discussions with and encouragement from Drs Greg Schoeppner of MLBC/AFRL, Tom Kim of AOARD/AFOSR. This research was sponsored by AOARD/AFOSR (Contract Number: F6256200M9220).

REFERENCES

1. Baker A A and Jones R. Bonded repair of aircraft structures. Martinus Nijhoff: Dordrecht; 1988
2. Baker A.A., Repair techniques for composite structures, Composite Materials in Aircraft Structures, Middleton D.H., Ed., Longman Scientific & Technical, 1990, Chapter 13, pp. 207-227
3. L.R.F. Rose, A cracked plate repaired by bonded reinforcement, Int. J. Fracture, 18, 135-144, 1982

4. L.J. Hart-Smith, The design of repairable advanced composite structures, Douglas Paper 7550, McDonnell Douglas, Douglas Aircraft Company, 1985
5. Adams R D Comyn J and Wake W C. 1997, *Structural Adhesive Joints in Engineering*, 2nd Edition. Chapman & Hall: London; 1997
6. Tong L and Steven G P. *Analysis and Design of Structural Bonded Joints*. Kluwer Academic Publishers: Boston; 1999
7. L. Tong & X. Sun, 'Stresses in bonded repair/joints to curved structures', US AFOSR/AOARD Contract Report FEARC-00-001, Jun 2000
8. L. Tong & X. Sun, Stress analysis of bonded and curved lap joints, Proceedings of American Society Composites 15th Technical Conference Sep 24-27, 2000, Edited by Ozden. O. Ochoa, Texas A&M University, USA, pp. 719-728
9. C. Zienkiewicz, The Finite Element Method, 4th ed. London, McGraw-Hill, 1990
10. R. H. Gallagher and O. C. Zienkiewicz, Optimum Structural Design Theory and Applications, London, John Wiley & Sons Ltd., 1973
11. J. G. Schoofs, L. H. Th. M. Van Buekering and M. L. C. Sluiter, 'triquamesh user's guide', Report WE 78-01, Eindhoven University of Technology, The Netherlands, Jan. 1978
12. J. A. Talbert and A. R. Parkinson, Development of an automatic, two-dimensional finite element mesh generator using quadrilateral elements and Bezier curve boundary definition, International Journal for Numerical Methods in Engineering, Vol.29, pp.1553-1267, 1990
13. Bogy DB, Two edge-bonded elastic wedges of different materials and wedge angles under surface tractions, Journal of Applied Mechanics, Vol. 38, 1971, pp.377-386
14. Erdogan F, Stress singularities in a two-material wedge. International Journal of Fracture Mechanics, Vol. 7, 1971, pp.317-330
15. Ning Hu, Bo Wang, Hideki Sekine, Zhenhan Yao and Guowen Tan, Shape-optimum design of a bi-material single-lap joint, Composite Structures, Vol.41, 1998, pp.315-330